Iranian Journal of Science and Technology, Transactions of Civil Engineering (2021) 45:2525–2554
https://doi.org/10.1007/s40996-020-00563-x

RESEARCH PAPER

Effects of Concrete Strength and Openings in Infill Walls on Blasting Responses of RC Buildings Subjected to TNT Explosive

Ahmet Can Altunışık[1] · Fatma Önalan[2] · Fezayil Sunca[3]

Received: 26 May 2020 / Accepted: 7 December 2020 / Published online: 18 January 2021

Abstract

The explosions caused by terrorism and/or accidental lead to serious damage and/or collapse in structures, economic losses, and most importantly endanger public safety. The blasting loads that can be larger than design loads are generally neglected in the design stage of civil engineering structures, despite these catastrophic effects. For these reasons, especially strategically important structures such as hospitals, military buildings, and bridges should be designed considering the blasting effects. To this aim, the effects of design parameters such as concrete strength and openings in infill walls on blasting responses of reinforced concrete (RC) buildings are investigated in this study. In situ experimental tests are firstly conducted on a test specimen constructed with brick elements to verify the finite element (FE) model criteria and assumptions. The blasting experiments are performed using 40, 150, and 290 g trinitrotoluene (TNT) explosives. Then, two RC buildings are selected as application, and blasting analyses are done with numerical and empirical methods. FE models of the buildings including structural and non-structural elements are constituted in ANSYS Workbench software. The blasting analyses are carried out with ANSYS AUTODYN software using 100 kg TNT explosives. In the analyses, two different openings in infill walls and six different concrete classes are considered. The blasting pressures, displacements, absorbed and released total energies, and damage ratios are obtained and presented as comparison parameters. The results obtained from the blasting analyses are presented with graphics and tables, comparatively. The study shows that peak pressures and maximum displacements decrease by 22.50% and 32.16% with the increase in concrete strength. Also, it is observed from numerical analyses that openings in infill walls lead to a change of 8.16% in peak pressures and 13.92% in maximum displacements.

Keywords Blasting · Concrete strength · Explosion · Infill walls · RC building · TNT explosive

1 Introduction

International economic problems and power imbalances cause an increase in terrorist activities. These activities usually target people directly or civil engineering structures such as strategically important buildings and bridges. On the other hand, gas stations close to settlements and factories containing explosive substances may also lead to destructive explosions. Although various static and dynamic loads (dead, live, snow, wind, earthquake, etc.) are widely used in the design stage of civil engineering structures, explosion-based loads and effects are generally neglected (Altunlu 2008). The explosions caused by terrorism and/or accidental lead to serious damage and/or collapse in structures, economic losses, and most importantly endanger public safety. Therefore, the design of structures resistant to blasting loads has become one of the most important civil engineering issues in recent years (Toy and Sevim 2017).

In the past years, blasting effects on structural behavior and performance have been investigated from many perspectives using experimental, numerical, and empirical methods. The first studies on blasting behavior began in the early part of the twentieth century, and these studies have accelerated

✉ Ahmet Can Altunışık
ahmetcan@ktu.edu.tr

Fatma Önalan
gulfatmaonalan@gmail.com

Fezayil Sunca
fsunca@cumhuriyet.edu.tr

[1] Department of Civil Engineering, Karadeniz Technical University, 61080 Trabzon, Turkey

[2] ASKİ General Directorate, 06050 Ankara, Turkey

[3] Department of Civil Engineering, Sivas Cumhuriyet University, Sivas, Turkey

since the mid-center of the twentieth century. Hopkinson and Cranz (1915) conducted the first important study to investigate the explosion effects. In addition, various empirical formulas have been proposed in the literature to calculate the several blasting parameters such as peak pressure, impulse, and durations. The empirical formulas represent the relationship between the blasting peak pressure and the scaled distances of detonations that are calculated using the distance of the explosion center and charge weight. Brode (1955) performed numerical solutions of spherical blast waves and identified blasting parameters such as positive and negative phase impulses and durations for various radial distances. Henrych and Major (1979) presented the empirical formulas using several experimental data to the calculation of explosion parameters. Kingery and Bulmash (1984) proposed a polynomial formulation to estimate blasting peak pressure and impulse. Kinney and Graham (1985), Mills (1987), and Sadovskiy (2004) proposed useful empirical formulas to the determination of parameters of the explosion such as peak pressure and durations based on scaled distance. As well as empirical formulas, advances in computer technology have enabled the use of hydrocodes such as AUTODYN AND LS-DYNA that provide realistic modeling of the explosion behavior.

In the literature, the effects of blasting on the structural behavior were handled for various engineering structures such as buildings and bridges. Therein, many aspects of the subject have been examined using numerical, empirical, and experimental methods. The structures were exposed to blasting materials and blast-induced ground motions in these studies. Luccioni et al. (2004) investigated the blast-induced structural failure of RC building and presented a comparison of the real damages of an existing building subjected to explosion and the damages obtained from numerical analysis. Jayasooriya et al. (2011) examined the impact of near-field explosions on the load-bearing system of RC buildings in order to be used in designing strategies to mitigate the total and progressive collapse of the structures. Tang and Hao (2010), Son and Lee (2011), and Hashemi et al. (2017) numerically simulated the effects of explosions on the behavior of cable-stayed bridge and its structural elements. Kelliher and Sutton-Swaby (2012) stochastically modeled the blast load damage levels of RC building. Yalciner (2014) revealed the role of corrosion on the blasting response of RC buildings. Coffield and Adeli (2015) investigated the resistance of irregular steel structures with different bearing system types against blasting loads. Andreou et al. (2016) proposed a modeling approach to the evaluation of the effect of explosions on bridges. Hacıefendioğlu (2017) performed stochastic analysis of a highway bridge exposed to blast-induced ground motion. Sevim and Toy (2019) conducted numerical analyses of an existing building exposed to the explosion for different charge weights. In the literature, some researches were conducted on the blasting behavior of various engineering structures such as historical buildings, walls, and art structures, as well as buildings and bridges (Wu et al. 2005; Wei and Stewart 2010; Yusof et al. 2014; Hacıefendioğlu and Koç 2016). Besides, various studies were carried out to reduce the blasting effects and damages (Wu et al. 2004; Tan and Patoary 2009; Hao and Tang 2010; Aoude et al. 2015; Zhang and Philips 2016; Codina et al. 2017).

The infill walls are generally considered as a non-structural element and widely preferred for various purposes in civil engineering structures (Furtado et al. 2020). However, when the infill walls are exposed to loads, they interact with the load-bearing systems of structures. This interaction can lead to different failure modes in infill walls (Furtado et al. 2015). In addition, the load-bearing system and infill wall interaction remarkably contribute to the structural performance of structures. Therefore, the contributions and effects of infill walls on the structural behavior, especially considering earthquake loads, are an attractive research area. In the literature, many aspects of the responses and behaviors of the infill walls have been examined using numerical and experimental methods, in recent years (Al Hanoun et al. 2018; Furtado et al. 2018; Onat et al. 2018; De Risi et al. 2019; Di Domenico et al. 2019; Onat, 2019; Cavaleri et al. 2020; Ricci et al. 2020). On the other hand, the contributions and effects of infill walls in the design phase of the structures subjected to the explosion are generally neglected. However, the damages and/or failures of the walls subjected to explosive materials may lead to high-speed debris or structural collapse and may cause significant life and economic losses (Li et al. 2017). For this reason, the roles of infill walls on the blasting behavior should be considered in the design and construction of structures that may be exposed to bursting loads. The many aspects of the blasting responses of the walls have been examined using different methods. The experimental studies that can accurately represent the detonation behavior of the walls are among the frequently preferred methods for the walls. In these experimental studies, blasting responses of the walls built with different masonry units were handled for brick (Zapata and Weggel 2008), for clay brick (Shi et al. 2016; Li et al. 2017), for London brick (Keys and Clubley 2017). In addition to the blasting behaviors of the walls built with different masonry units, the strengthening materials were investigated to increase the blasting resistance of the walls. Davidson et al. (2004) and Chen et al. (2020) conducted experimental studies on the sprayed-on polymers to increase the blast resistance of the walls and panels. Besides, the fiber reinforced polymers such as carbon fiber reinforced polymer (CFRP) and glass fiber reinforced polymer (GFRP) were used by researchers to improve the detonation resistance of the walls and panels (Alsayed et al. 2016; Chen et al. 2020).

In this study, the effects of concrete strength and openings in the infill walls on blasting responses of RC buildings are investigated using numerical and empirical methods. In situ experimental tests are firstly carried out to verify the FE model criteria and assumptions. For this purpose, a test specimen was constructed using brick elements. The hollow ratio of the brick elements was determined in accordance with the requirements of the Turkish Earthquake Code (TEC 2018). The upper surface of the test specimen was constructed completely open to the atmosphere in order to compensate complex effects of blasting. The blasting experiments were executed using 40 g, 150 g, and 290 g capsule sensitive TNT explosives on the inner base center of the specimen. Then, two RC buildings are selected as application. FE models of the RC buildings are constituted in ANSYS Workbench (2016). The blasting analyses are carried out by using ANSYS AUTODYN (2016). The blasting pressures, displacements, absorbed and released total energies, and damage ratios are selected as comparison parameters. Moreover, the blasting peak pressure values are calculated by using empirical formulas purposed by Brode (1955) and graphs given in "Structures to Resist the Effects of Accidental Explosions" (UFC 3-340-02 2008). Figure 1 shows the flowchart of the study. The results show that the blasting responses of load-bearing systems and infill walls are changed significantly due to concrete strength and opening in infill walls.

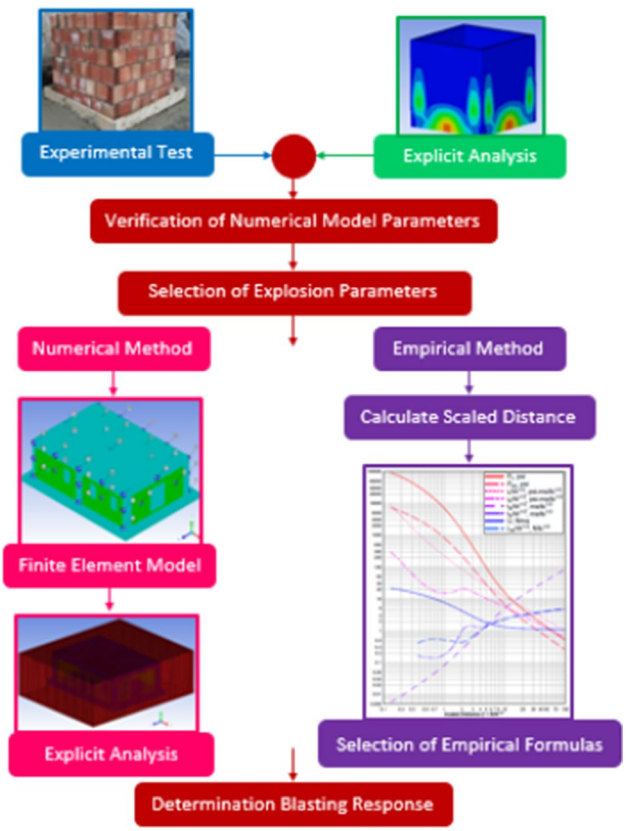

Fig. 1 The flowchart of the study

2 Blast Theory

The detonation of high-intensity explosives leads to blast waves. The blast waves produce a shock wave effect that spreads from the explosion center to the atmosphere with hemispherical form. After the shock wave releases from the center of the explosion, it reaches the maximum pressure (P_{so}) and speed value in a short time like a millisecond. As the shock wave moves away from the explosion center, the surface area expands and the pressure value gradually decreases. This process continues until a balance is achieved with the air surrounding the shock wave. This process is defined as the positive phase duration (t_o). During the propagation of the shock wave, the pressure value in the region behind of the shock wave falls below the ambient pressure and creates negative pressure (P_{so}^-). This process, which creates a vacuum effect, is defined as the negative phase duration (t_o^-). The time-history graph of blast wave pressure is given in Fig. 2.

In front of the shock wave, the air in the environment compresses according to the movement direction of the wave and moves together with the shock wave like a set. Thus, it creates a much larger positive pressure compared to the ambient pressure. This positive pressure in front of the shock wave is considerably higher than the negative pressure behind it. The negative phase duration is longer but less effective than the positive phase duration. It can be seen from the literature that the positive peak pressure that occur during the positive phase duration causes most

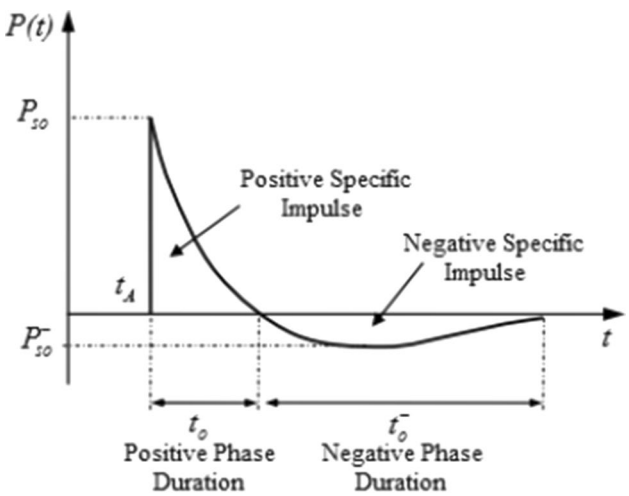

Fig. 2 Evaluation of blast wave pressure (Ngo et al. 2007)

of the damages in the structures and the negative pressure is neglected.

The explosions can be classified from various perspectives such as explosive substances and the blasting waveforms (Ullah et al. 2017). In general, these can occur in four main types: physical, chemical, electrical, and nuclear detonations. The environment in which the explosion occurs affects the explosion waves and the explosions can also be classified in this respect: free air blast, airburst, surface burst, fully vented, partially confined, and fully confined (UFC 3-340-02). The explosion responses of the buildings determine by using numerical, experimental, and empirical methods. Although experimental methods provide the realistic results, they are generally not preferred due to the dangers, difficulties, and formal procedures. In addition, it is impossible to conduct experiments in structures for all types of explosives. Therefore, empirical formulas used to estimate the parameters of large-scale explosions for various distances and charge weights can be preferred. Many empirical formulas for detonation parameters have been presented in the literature. In most of these, detonation parameters such as peak pressure and positive phase duration are identified with the scaled distance. The scaled distance (Z) calculates by using Eq. (1). In Eq. (1), R is an explosion distance between structure and explosion center (m) and W is the mass of explosive substances expressed in TNT explosive (kg).

$$Z = \frac{R}{\sqrt[3]{W}} \tag{1}$$

In this study, the maximum pressures were obtained with the empirical formula proposed by Brode (1955) and the graph given in UFC 3-340-02. These pressures were compared with the FE analyses results. The formulas purposed by Brode in 1955 for calculation of peak pressure based on the scaled distance are presented with Eq. (2).

$$P_{so} = \frac{6.7}{Z^3} + 1 \qquad for\, P_{so} > 10bar$$
$$P_{so} = \frac{0.975}{Z} + \frac{1.455}{Z^2} + \frac{5.85}{Z^3} - 0.019 \quad for\, 0.1bar < P_{so} < 10bar \tag{2}$$

In the design of the structures, the graphs are presented by UFC 3-340-02 to determine the shock wave parameters of several blasting types. The graph of the positive phase shock wave parameters for a spherical TNT explosion from free air bursts is given in Fig. 3. In this graph, parameters such as peak pressure, reflected pressure, impulse, and velocity can be obtained depending on the scaled distance. In Fig. 3, L_w, P_r, and U are the wavelength of positive pressure phase, peak positive normal reflected pressure, and shock velocity. Besides, i_r, i_s, t_a, and t_o are represented reflected impulse, incident impulse, time of arrival of the blast wave, and duration of blast pressure, respectively.

3 Experimental Tests

To determine the blasting response of structures, the experimental tests are not frequently preferred due to measurement costs, construction difficulties, risks, and formal procedures. For this reason, comparative studies are generally conducted using numerical and empirical methods in the literature. In this section, the experimental tests were carried out to verify the FE model. For this purpose, a test specimen was constructed using brick elements and blasting tests were conducted considering various charge weights which lead to different damage levels of the walls. Throughout this section, detailed information about the test specimen such as material properties and geometric dimensions was firstly presented. Then, details of the blasting test protocols and explosive substance to be used in the tests were described.

3.1 Specimens' Detailing

According to the TEC, 2018, the hollow ratio of the brick elements was chosen as 45%. The material properties of the selected brick elements are given in Table 1. The width, length, and thickness of each masonry wall are 122 cm, 113 cm, and 8.5 cm, respectively. The mortar thickness was selected as 10 mm. While creating the test specimen, it is aimed to compare the experimental results with the numerical results and to show the accuracy of the parameters considered in numerical analysis. For this reason, a special scale coefficient was not taken into consideration and the simplest model features were used. The upper surface of the constructed model is completely open to the atmosphere. The wall supports were embedded in the foundation to prevent translations and rotations. The blasting loads have complex effects on the structures. If the slab and different boundary conditions are considered during the experiments, a variety of details such as the behavior of slab to wall connection and soil–structure interaction should be taken into account in the numerical analyses. This situation can cause the blasting effects on the wall to be more complex. For this reason, the complexity of structural behavior was reduced with these conditions that were considered during the experiments. The dimensions and photographs of the test specimen are given in Fig. 4.

3.2 Test Methodology

Blasting tests were carried out 28 days after the walls construction to gain sufficient strength of mortars. During the experiments, 40 g, 150 g, and 290 g capsule sensitive TNT

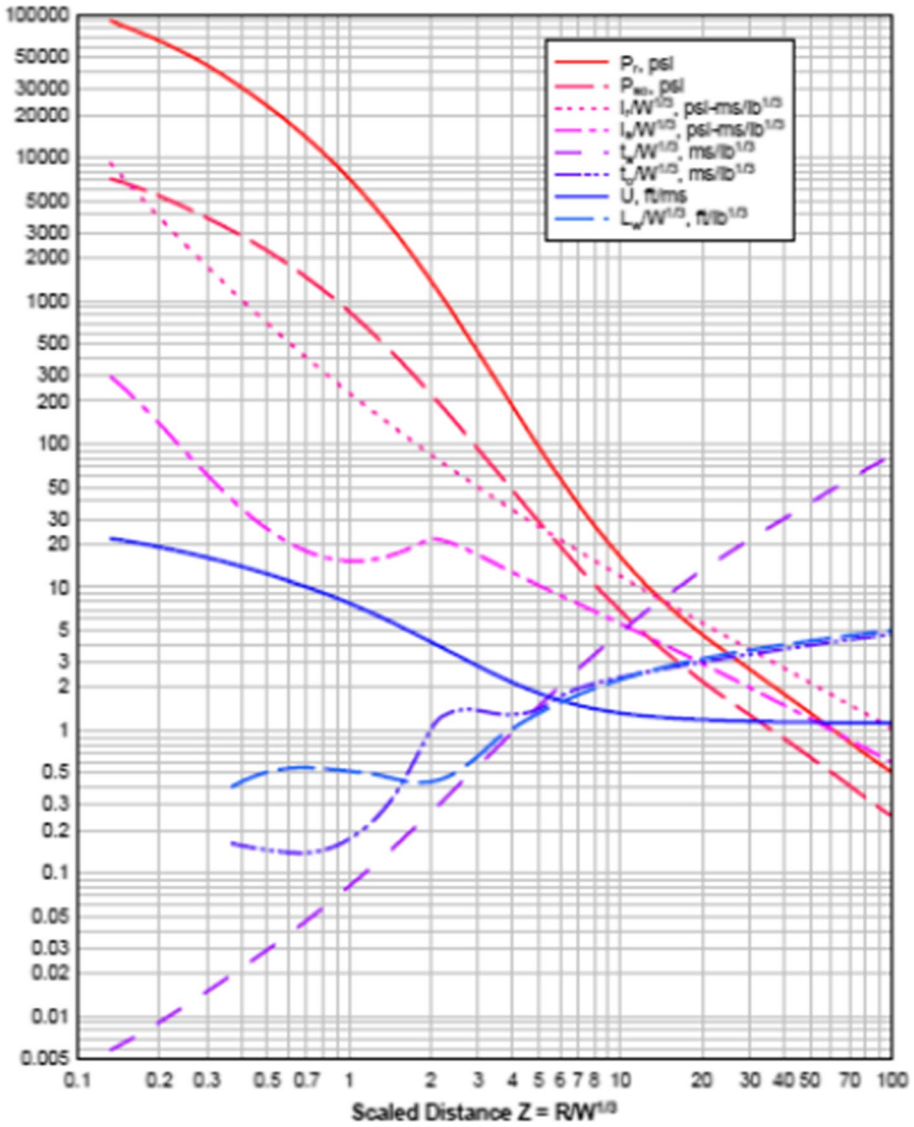

Fig. 3 Positive phase shock wave parameters for a spherical TNT explosion from free air bursts (UFC 3-340-02 2008)

Table 1 Material properties of the selected brick elements

Material	Modulus of elasticity (MPa)	Density (g/cm^3)	Compressive strength (MPa)
Brick	2.88×10^3	0.69	0.8

explosives were preferred to evaluate progressive blast damage of the test specimen. These charge weights were taken into consideration to investigate the blasting responses and behaviors of the wall in undamaged, damaged, and collapsed situations. The explosive substances were placed on the inner base center of the specimen. The TNT explosives were covered with a layer of sand to prevent the explosive from spreading around due to high pressure. The tests were performed by monitoring the damages levels without measurement devices, thanks to the selected explosive substance weights. Figure 5 presents the experimental setup and selected TNT explosives.

3.3 Experimental Blasting Test Results

In the blasting tests performed with 40g TNT explosive, micro-cracks which provide the immediate occupancy performance level were monitored. The damages on the wall were also developed with the increase in the charge weight from 40 to 150 g. During the blasting tests carried out with 290 g TNT explosives, it was seen that the walls collapsed by separating from supports. Moreover, it was observed that the brick fragments spread to the environment at high speed due to the high-pressure effect caused by blasting. This situation clearly shows that if the necessary security measures are not taken during the blasting tests, serious dangers may occur for the safety of life and property. Figure 6 shows the

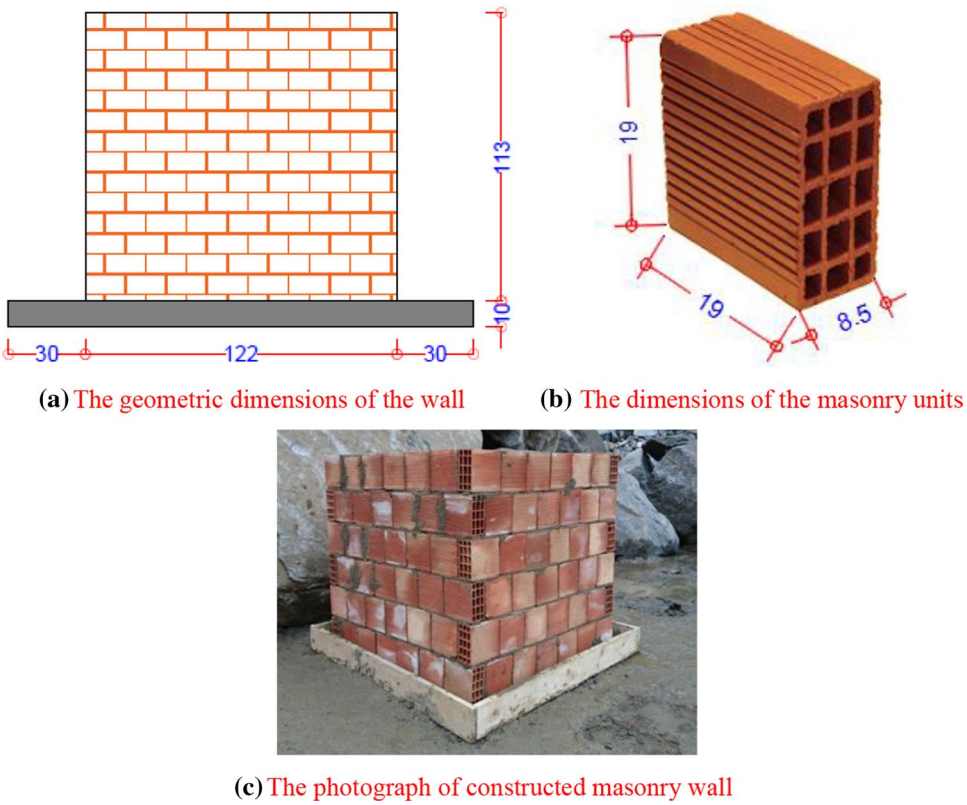

Fig. 4 The constructed test specimen for blasting tests (all dimensions in cm)

(a) The geometric dimensions of the wall **(b)** The dimensions of the masonry units

(c) The photograph of constructed masonry wall

Fig. 5 The selected capsule sensitive TNT explosive and blasting test setup

Fig. 6 The collapsed masonry walls after blasting test performed with 290 g TNT explosive

collapsed masonry walls after the blasting test performed with 290 g TNT explosive.

3.4 FE model of the Test Specimen

FE model of the test specimen walls was constituted using the explicit dynamic analysis section in ANSYS Workbench. The blasting analyses were performed in ANSYS AUTODYN. The Lagrange theory that includes calculations for the conservation of mass, energy, and momentum was used for solid elements. Air volume and TNT explosives were modeled according to Euler's theory. The macro-modeling approach was selected for the FE model of the walls. Mesh sizes were chosen as 100 mm for solid elements and 15 mm for air and TNT explosives as a result of the mesh converge analyses. During the experimental tests, the wall supports were embedded in the RC foundation to prevent translations and rotations. Therefore, fixed boundary condition was assumed at the bottom surfaces of the masonry walls. The 3D FE model of the masonry walls and the location of the TNT explosive are given in Fig. 7.

The analysis duration and time increment were taken as 3 ms and 0.01 ms to observe the pressure changes, precisely. In blasting analysis, suitable material properties and models should be selected to measure the overloads occurring within milliseconds. To this aim, Riedel–Hiermaier–Thoma (RHT) model (Riedel et al. 1999) was selected for brick and concrete in this study. This model has been experimentally tested on test specimens subjected to impulsive loads and has been determined to adequately reflect concrete material behavior during the explosion. Moreover, the P-alpha (Hermann 1969) equation of state was used for brick material. The air volume containing the brick elements and TNT explosives was modeled as ideal gas equation of state. The air is a gaseous substance and stress in itself is not occur. The air volume, which is not affected by fracture and principal stress changes, serves as a material that transfers stresses caused by the explosion. For the air volume, the density, room temperature, specific temperature, and threshold energy were used as 1.25×10^{-3} g/m^3, 288.20 K, 717.59 J/kg K, and 2.07×10^5 kJ/kg, respectively. In the numerical model of the wall, the TNT explosives were represented using the Jones–Wilkens–Lee (JWL) equation of state. This equation of state, which is described by using the various parameters such as hydrostatic pressure, density, and the specific internal energy corresponding to the unit weight of TNT, reflects the properties of rapid expansion and diffusion, accurately. For the TNT explosives, the density, threshold energy, velocity, energy, and pressure of the blasting were used as 1.63 g/m^3, 3681 kJ/kg, 6930 m/s, 6×10^6 kJ/m^3, and 2×10^4 MPa, respectively. Table 2 summarizes the material properties and equations considered in analyses.

As a result of blast analyses, damage contour diagrams and maximum pressure values were obtained. The maximum pressure values were measured as 341 kPa at 0.50 ms for 40 g TNT explosive and 867 kPa at 0.41 ms for 150 g TNT explosive. As a result of analysis with 290 g TNT explosives, maximum pressure was obtained as 1590.7 kPa at 0.37 ms. The pressure value of 1590.7 kPa is considerably greater than the allowable stress of brick elements. This situation shows that similar to experimental tests, the masonry walls are completely demolished with 290 g TNT explosive. Also, it was revealed that the FE model was correctly constituted. The damage contour diagrams obtained for each scenario are given in Fig. 8.

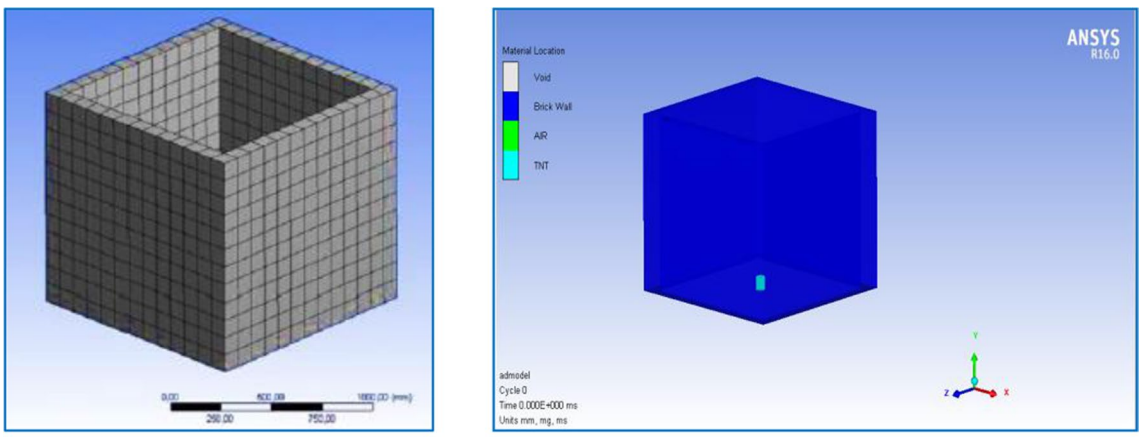

(a) FE model of the wall (b) The location of TNT explosive

Fig. 7 The 3D FE model of the masonry walls and the location of blasting material

Table 2 Material properties and equations of state considered in the blasting analyses

Material	Equation state	Strength model	Density (g/cm^3)	Shear modulus (MPa)	Elasticity modulus (MPa)	Compressive strength (MPa)
Brick	P-alpha	RHT	0.69	1.19×10^3	2.88×10^3	0.8
Air	Ideal gas	–	1.225×10^{-3}	–	–	–
TNT	JWL	–	1.63	–	–	–

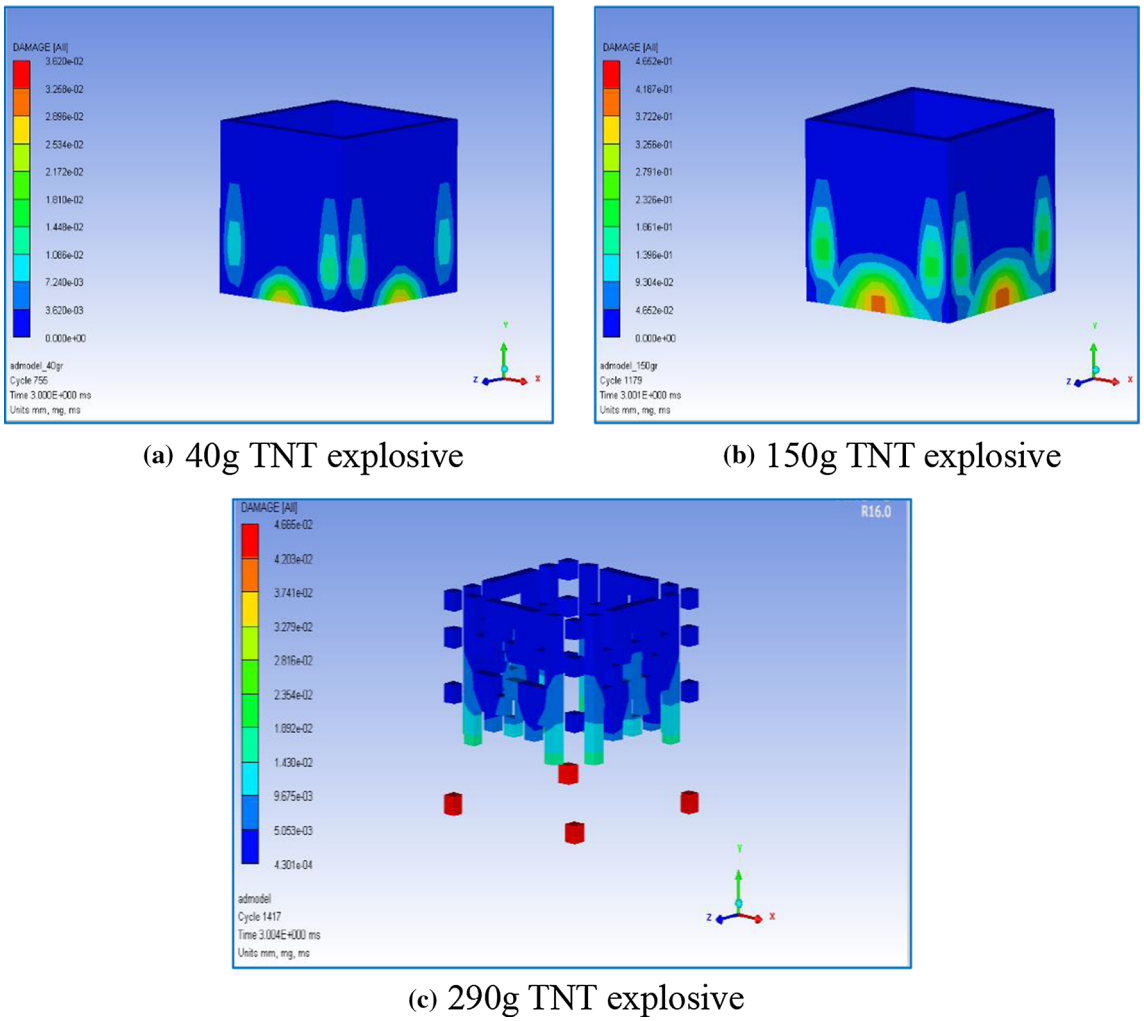

(a) 40g TNT explosive

(b) 150g TNT explosive

(c) 290g TNT explosive

Fig. 8 Damage contour diagrams of test specimen for different blast scenarios

4 Numerical Application

In this section, two RC building models were selected as an application to investigate the effects of concrete strength and openings in the infill walls on blasting responses. For these purposes, different opening ratios in the infill walls of the building models were taken into account, during the blasting analyses. Moreover, C25/30 ($f_{ck}=25$ MPa), C30/37 ($f_{ck}=30$ MPa), C35/45 ($f_{ck}=35$ MPa), C40/50 ($f_{ck}=40$ MPa), C45/55 ($f_{ck}=45$ MPa), and C50/60 ($f_{ck}=50$ MPa) concrete classes were used in the analyses to investigate the concrete strength effect on blasting behavior. The explosion material was selected as 100 kg TNT, and it was placed at the

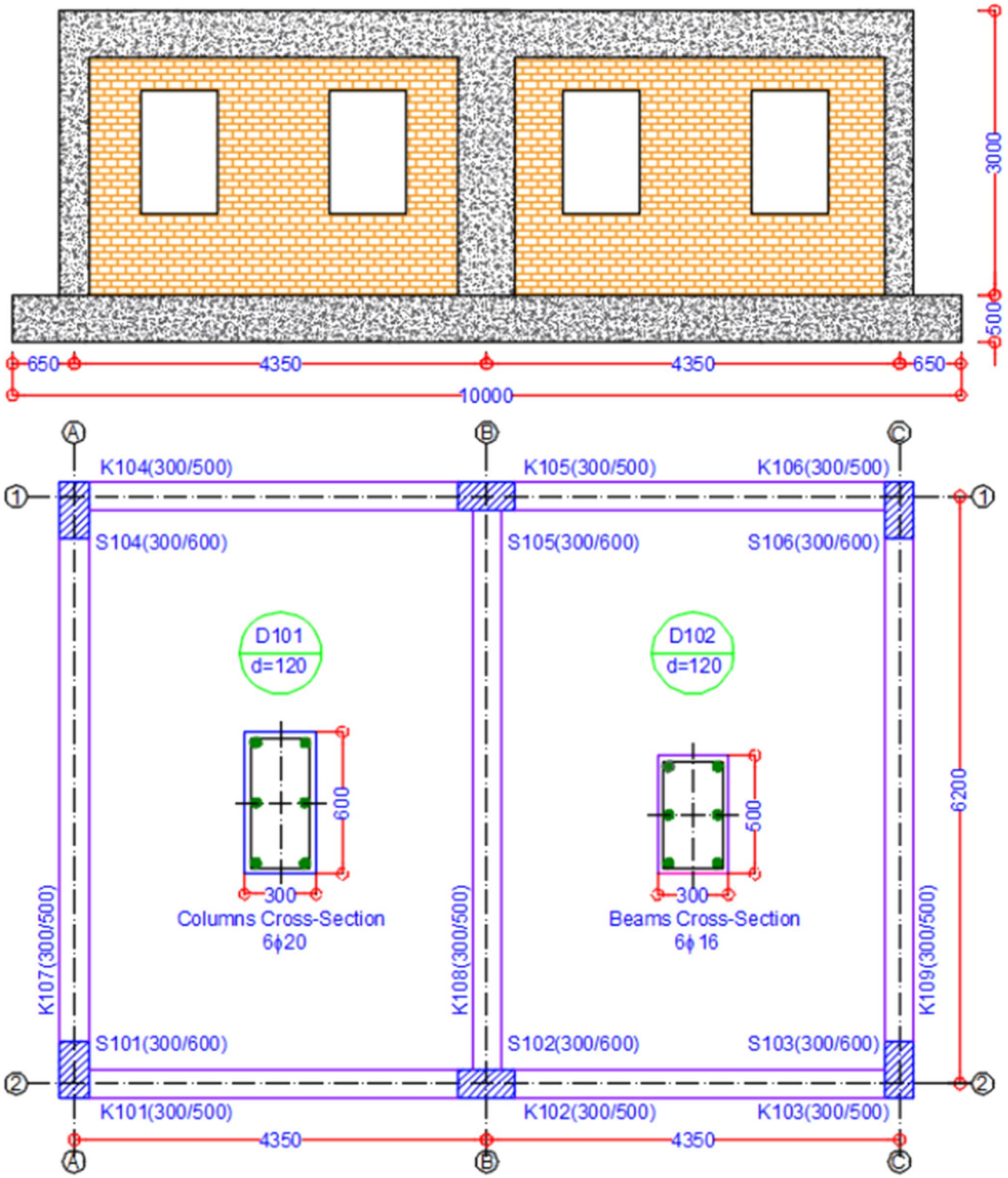

Fig. 9 The 2D views of the RC buildings and the cross sections of the structural elements (all dimensions are in mm)

façade of the buildings. The TNT explosive was defined 0.5 m away from the buildings. Besides the numerical analyses, the maximum pressure values caused by the explosion are calculated using the empirical formula proposed by Brode (1955) and the graph given in UFC 3-340-02 2008.

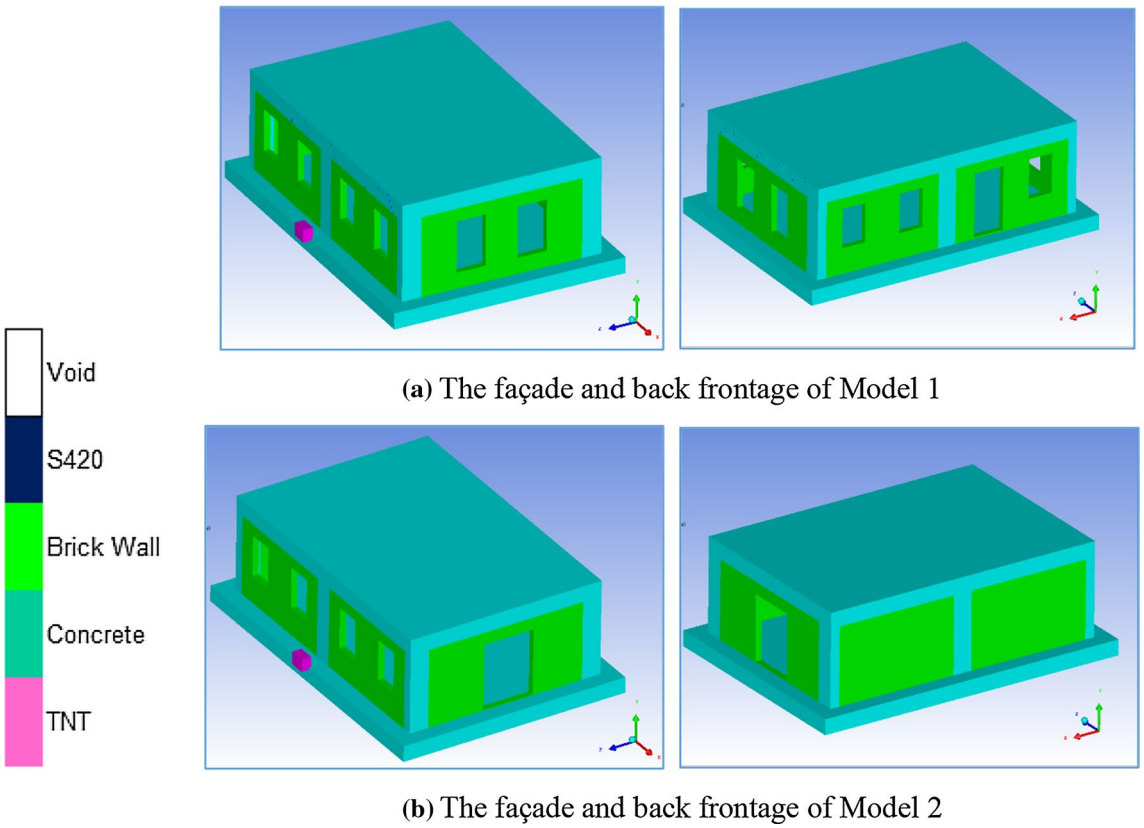

Fig. 10 The FE model of the building models

Table 3 The selected material parameters and mechanical properties of concrete material

Concrete class	Equation state	Strength model	K MPa	E_c	G_c	f_{ck}	f_{ctk}
C25/30	P-alpha	RHT	1.67×10^4	3.0×10^4	1.25×10^4	25	1.8
C30/37			1.78×10^4	3.2×10^4	1.33×10^4	30	1.9
C35/45			1.94×10^4	3.3×10^4	1.46×10^4	35	2.1
C40/50			2.22×10^4	3.4×10^4	1.67×10^4	40	2.2
C45/55			2.50×10^4	3.6×10^4	1.88×10^4	45	2.3
C50/60			2.78×10^4	3.7×10^4	2.08×10^4	50	2.5

Table 4 The properties of reinforcing steel, brick, air volume, and TNT explosives

Parameter/material		S420	Brick	Air volume	TNT
Equation state		Linear	P-alpha	Ideal gas	JWL
Strength model		Johnson–Cook	RHT	–	-
Density	g/cm^3	7.83	0.70	1.225×10^{-3}	1.63
Bulk modulus	MPa	1.67×10^5	–	–	–
Elasticity modulus		2.00×10^5	3.75×10^3	–	–
Shear modulus		7.69×10^4	1.19×10^3	–	–
Tensile strength		420.00	1.00	–	–
Compressive strength		420.00	5.00	–	–
Room temperature	K	300	–	288.20	–
Specific heat	J/kgK	477	–	717.59	–
Threshold energy	kJ/kg	–	–	2.07×10^5	3681.00
Detonation velocity	m/s	–	–	–	6930.00
Detonation energy	kJ/m^3	–	–	–	6.00×10^6
Detonation pressure	MPa	–	–	–	2.00×10^4

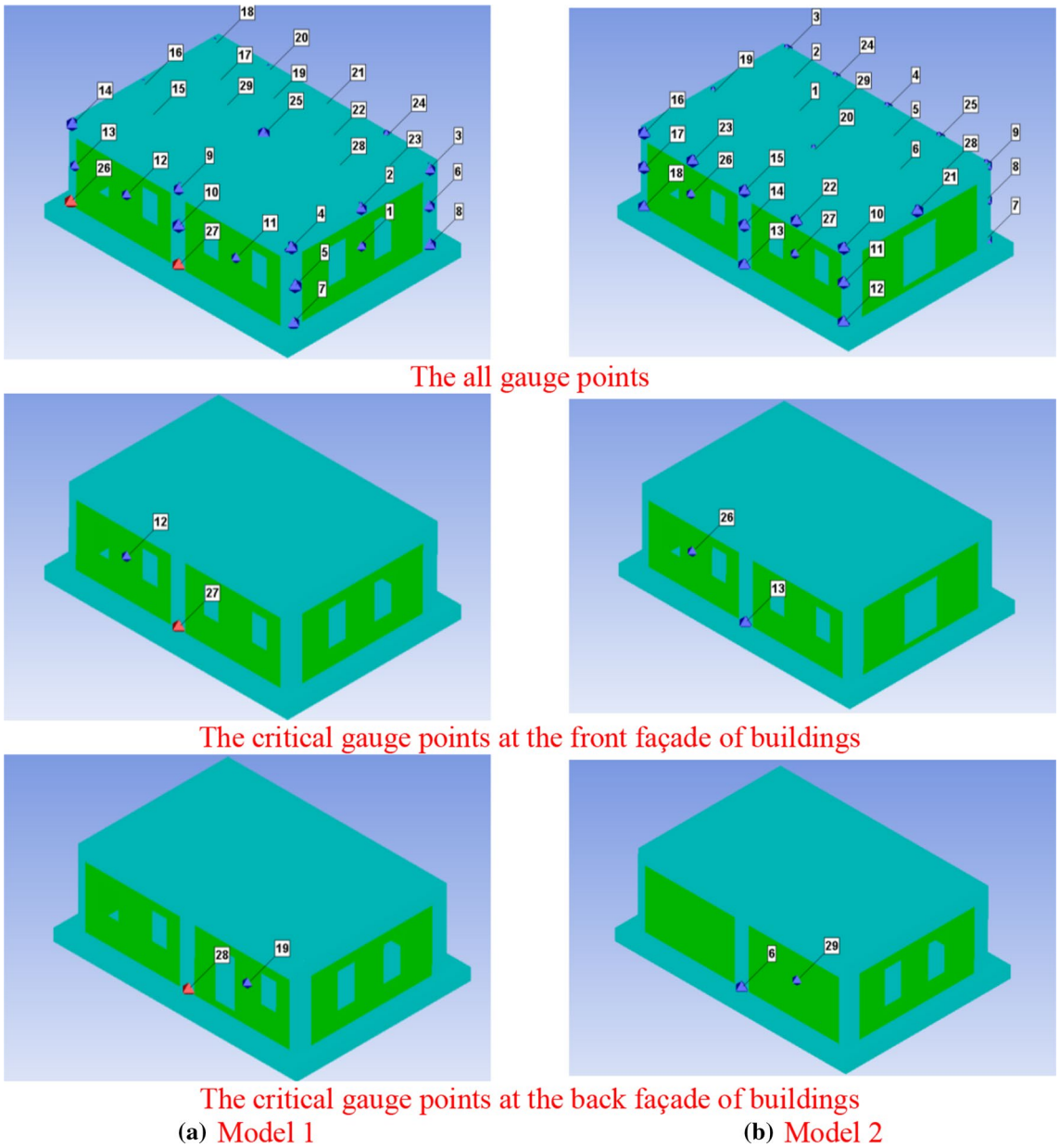

Fig. 11 The selected gauge points for RC building models

The load-bearing frame of the RC buildings was formed with high ductile moment frames. The buildings were designed according to the requirements of the Turkish Standard 500 (TS500, 2000) and TEC 2018. The building models have two bays in the x-direction with 4.50 m and one bay in the z-direction with 6.20 m. The height of the structures is 3.00 m. The cross-sectional dimensions of the columns and beams are 60 × 30 cm and 50 × 30 cm, respectively. The slab thickness is selected as 12 cm. The reinforcing steel class is considered as S420 (f_{yk} = 420 MPa). Longitudinal bars in all columns and all beams are calculated as 6ϕ20 and 6ϕ16, respectively. The confinement bars in all columns are ϕ8/100 mm for the confinement zone and ϕ8/195 mm for others. Moreover, the confinement bars in all beams are ϕ8/100 mm for the confinement zone and ϕ8/200 mm for others. The geometrical dimensions, plan views of the selected RC buildings, and cross sections of structural elements are shown in Fig. 9.

FE models of the buildings were constituted using ANSYS Workbench and were transferred into ANSYS AUTODYN to perform explicit analyses. The Lagrange theory was used for solid elements. Air volume and TNT explosives were modeled according to Euler's theory. To observe the homogeneous distribution of the explosion

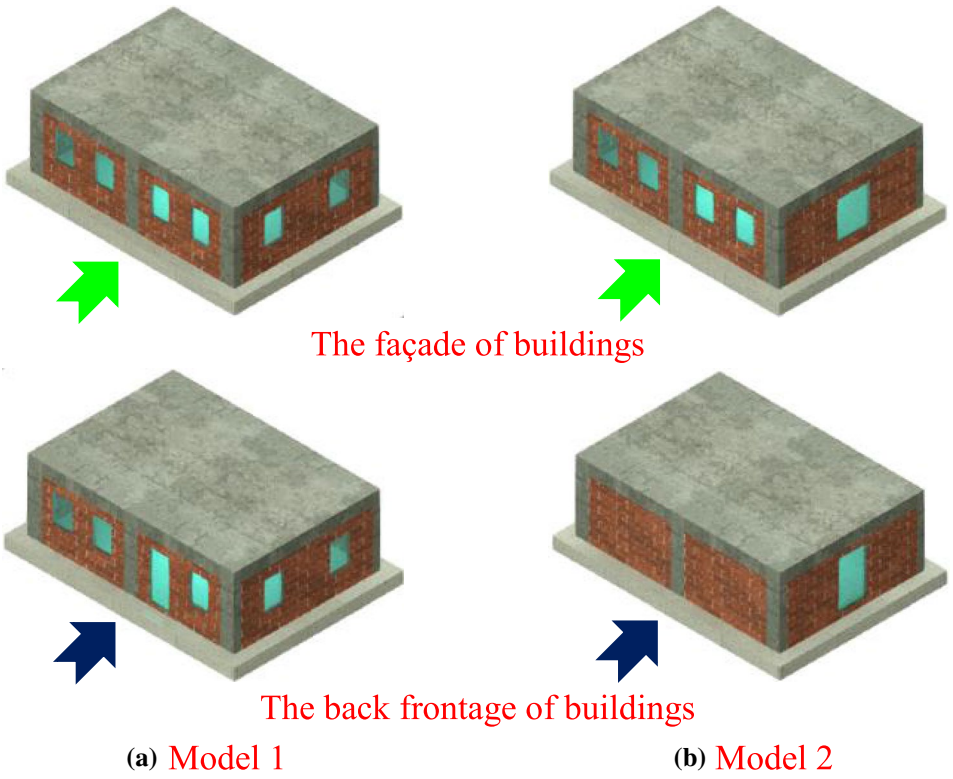

	Total infill area (m^2)	Total opening area (m^2)	Opening ratio (%)
Model 1	70.00	15.14	21.63
Model 2	70.00	10.40	14.86

Fig. 12 The opening ratios in the infill walls of all frontages

effects on the structure, an air volume was constituted, and the buildings were placed symmetrically in the center of air volume. Therefore, the dimensions of the air volume were calculated as 11 m × 4.5 m × 13.2 m in the *x*, *y,* and *z* directions, respectively. The mesh sizes were chosen as 100 mm for air and TNT explosives. The FE model of the buildings is given in Fig. 10.

In blasting analysis, suitable material properties and models should be selected to measure the overloads occurring within milliseconds. To this aim, the RHT model was selected for concrete material. Moreover, the P-alpha equation of state was used for concrete material. During the blasting analyses, the selected material parameters and mechanical properties for concrete material are given in Table 3. In addition, the Poisson ratio and weight per unit volume for all concrete classes are selected as 0.2 and 2.4 g/cm^3, respectively. In Table 3, K, E_c, G_c, f_{ck}, and f_{ctk} are the bulk modulus, elasticity modulus, shear modulus, compressive strength, and tensile strength of concrete, respectively.

The reinforcing steel was considered as linear elastic, isotropic, and strain hardening. Johnson–Cook model (Johnson and Cook 1983) was used for the plastic response of reinforcing steel. The linear equation of state was used for steel material. The air volume containing the structures and explosives was modeled as the ideal gas equation of state. The JWL equation of state, which accurately reflects the properties of rapid expansion and diffusion, was selected for TNT explosives. The selected properties for reinforcing steel, brick, air volume, and TNT explosive are summarized in Table 4.

In the blasting analyses performed with 100 kg TNT explosive, 29 gauge points for buildings were specified to monitor the displacements, pressures, damages, and total energies. In order to obtain the structural responses occurring at the different scaled distances and different facades of buildings, gauge points were placed in various specific points on all facades of the buildings including joints of the load-bearing system elements, structural elements-infill wall interaction regions, areas close to opening in infill walls. The

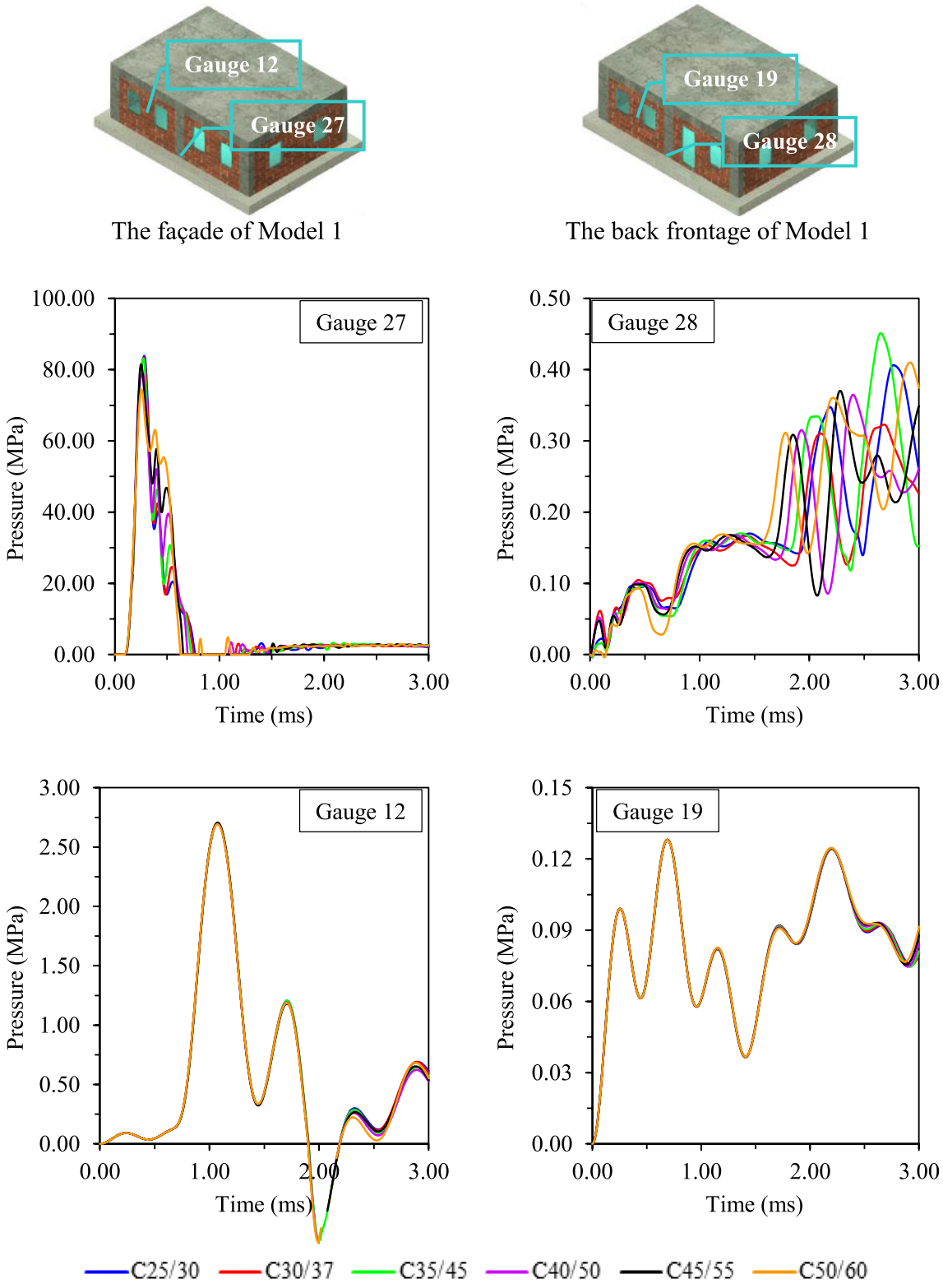

Fig. 13 The time-histories of pressures obtained from critical gauges of Model 1

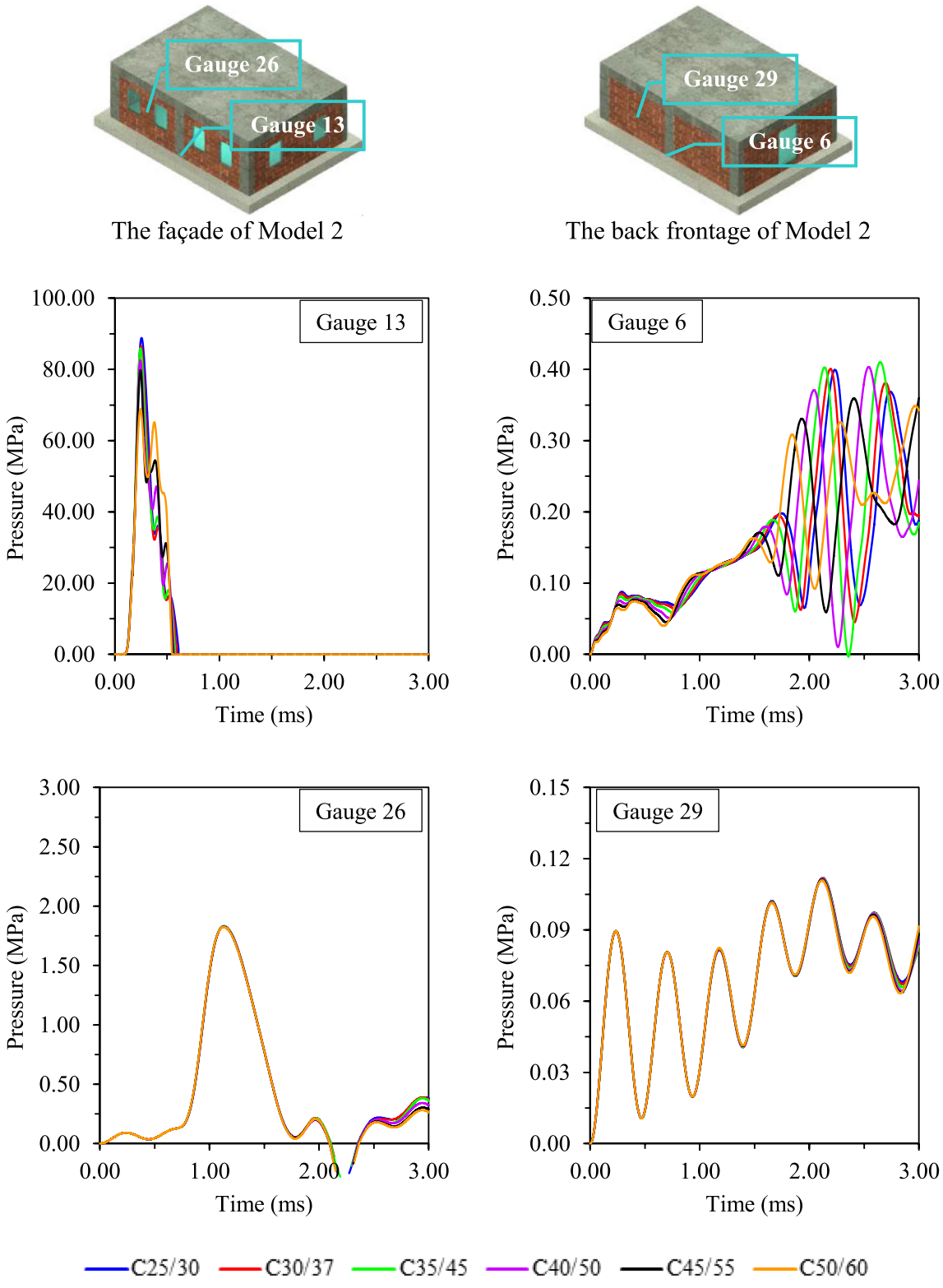

Fig. 14 The time-histories of pressures obtained from critical gauges of Model 2

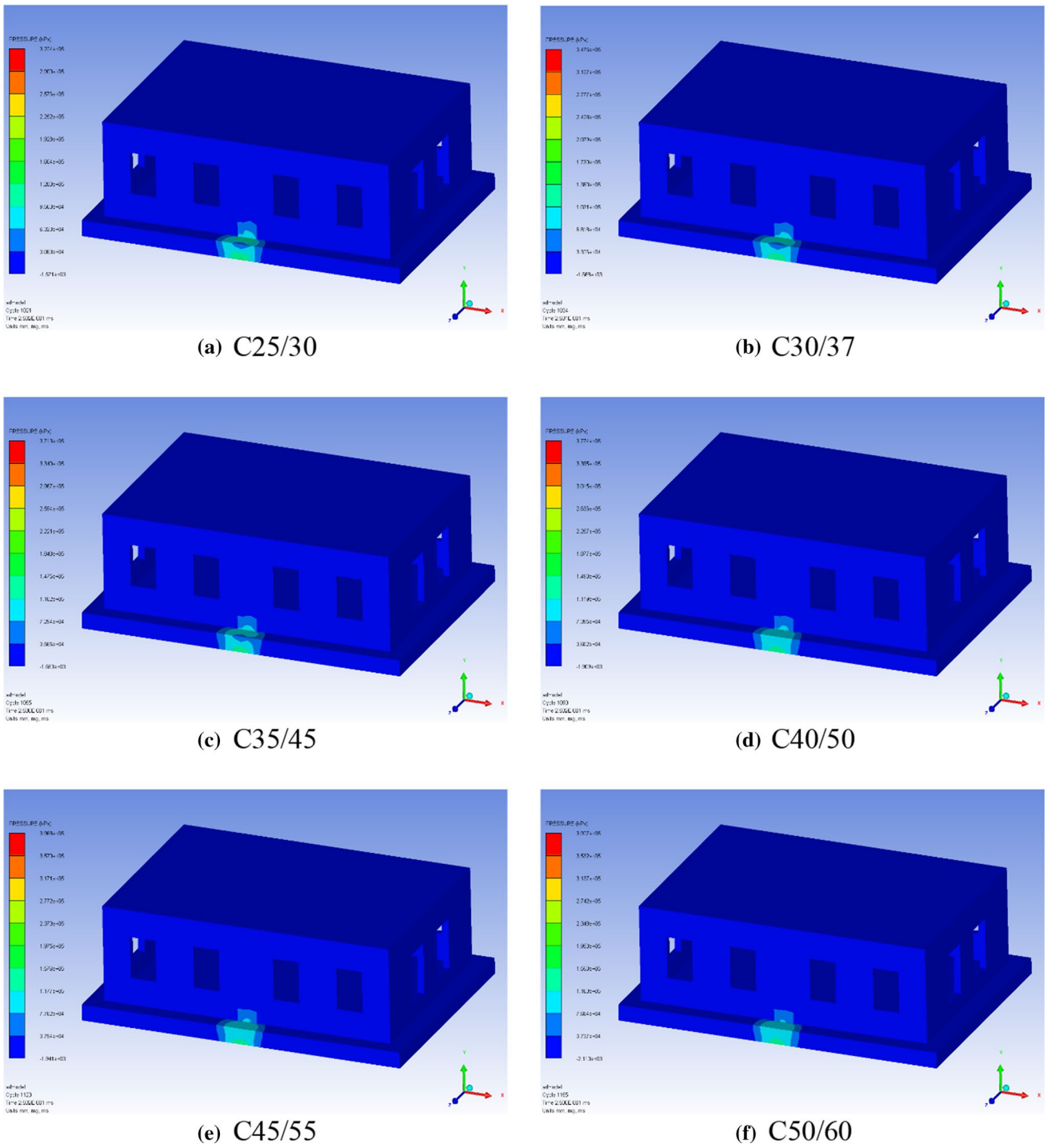

Fig. 15 The pressure contour diagrams obtained from 100 kg TNT explosive for Model 1

structural responses of the models obtained from all gauge points were comparatively analyzed to accurately monitor the effects of concrete strength and openings in infill walls on blasting responses of the buildings. As a result of the comparisons, the critical gauge points where the maximum structural responses were obtained in both the load-bearing system and the infill walls were determined. The maximum responses were obtained from the gauge 27 for Model 1 and gauge 13 for Model 2. The gauges 27 and 13 are located on the façades of buildings and are closest to the explosion

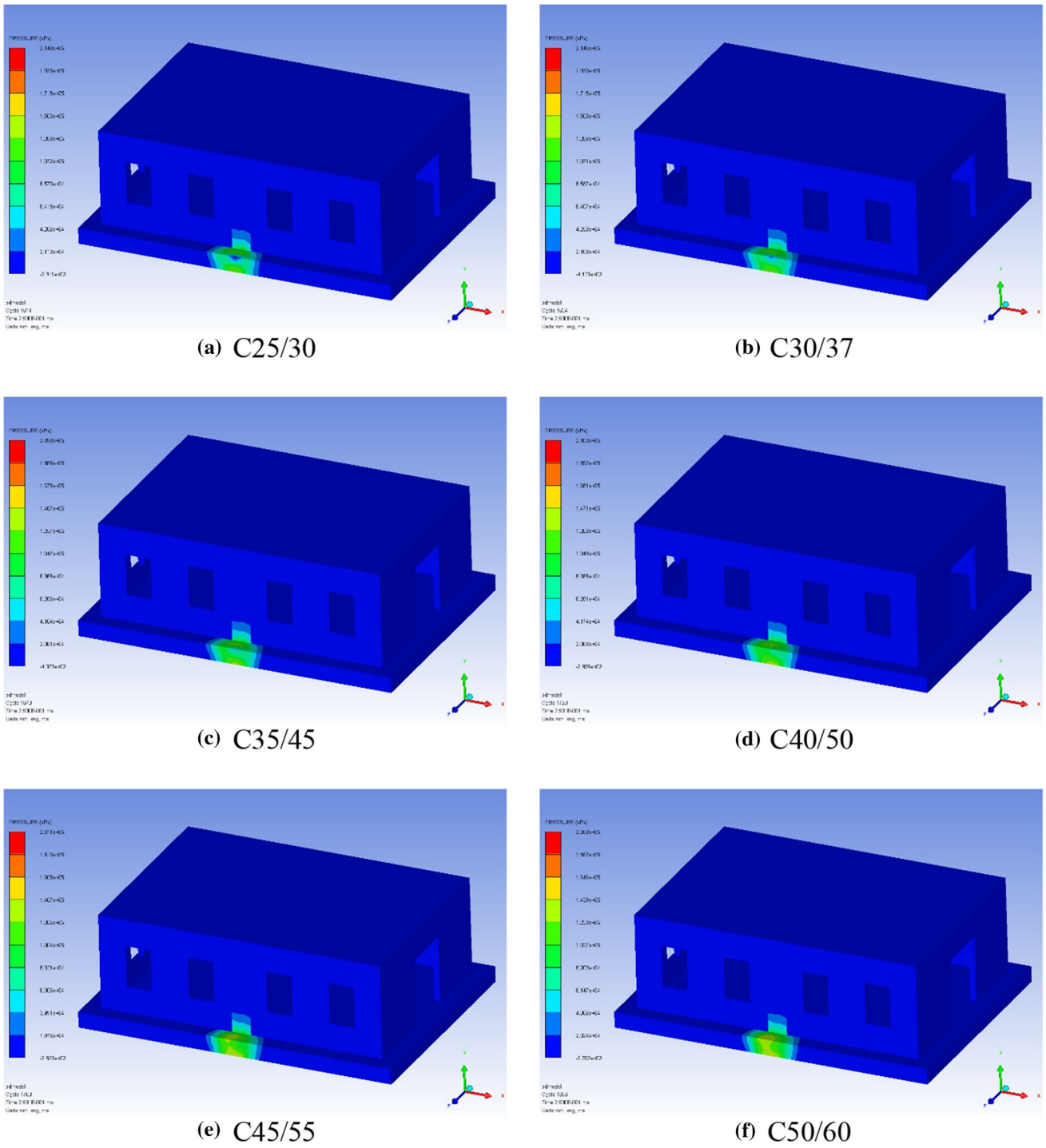

Fig. 16 The pressure contour diagrams obtained from 100 kg TNT explosive for Model 2

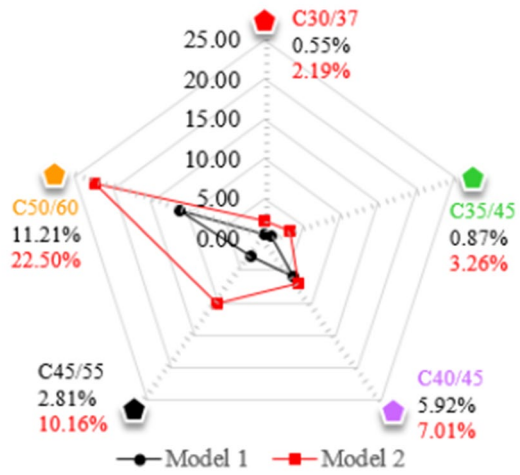

Fig. 17 The decreases (%) in peak pressures of Model 1 and Model 2 due to the increased concrete strength according to the C25/30

center. Similarly, the maximum responses in the infill walls are obtained from the façades of buildings, and these gauge points were determined as gauge 12 for Model 1 and gauge 26 for Model 2. In addition to the gauge points on the façade of the buildings, critical gauge points of both the load-bearing system and the infill walls (gauge 19, gauge 28 for Model 1 and gauge 6, gauge 29 for Model 2) were also determined on the back frontage to observe the effects of openings in infill walls on blasting responses. In the further sections of the study, the results obtained from the critical gauge points were investigated, comparatively. These all gauge points and determined critical gauge points are given in Fig. 11.

5 Evaluation of Blasting Analyses Results

This study is focused on the evaluation and comparison of concrete strength and openings in the infill walls effects on blasting responses of RC buildings. To this aim, two building models that have different opening ratios in the infill walls were taken into account, during the blasting analysis. In Model 1, openings were designed on the infill walls of all frontages so that the pressure caused by the explosion can easily enter and exit the building. In Model 2, the infill walls of the back frontage were considered as without openings. The other characteristics of the buildings were designed to be the same in order to make an accurate comparison. The openings in the infill walls are given in Fig. 12. During the blasting analyses, concrete strength was also used as an analysis parameter. To evaluation of the blasting analysis results, the pressures, displacements, absorbed and released total energies, and damage ratios obtained from blasting analysis were selected as comparison parameters. Four critical gauge points located on the façade and back frontage of building models were selected to evaluate these effects more clearly.

To monitor the concrete strength effects on blasting responses, the time-histories of pressures at the all frontage for Model 1 and Model 2 are presented in Figs. 13 and 14. The pressure contour diagrams in the time step when the peak pressure is obtained are given in Figs. 15 and 16. The decreases in peak pressures with the increasing concrete strength were calculated based on C25/30 and presented in Fig. 17. It is shown from Figs. 13, 14, 15 and 16 that the peak pressures are found at the gauge 27 for Model 1 and gauge 13 for Model 2. The gauges 27 and 13 are located on the façades of buildings and are closest to the explosion center. Similarly, the peak pressures in the infill walls are obtained from the façades of buildings (gauge 12 for Model 1 and gauge 26 for Model 2). With the increase in concrete strength from C25/30 to C50/60, the peak pressure values decreased from 83.85 MPa to 74.45 MPa for Model 1 and 88.81 MPa to 68.83 MPa for Model 2. It can be seen from Fig. 17 that the peak pressures decrease by 11.21% for Model 1 and 22.50% for Model 2 with the increasing concrete strength. Moreover, the peak pressures in the infill walls of Model 1 and Model 2 are found as 2.70 MPa and 1.82 MPa for all concrete classes, respectively. These situations point out that the concrete strength is considerably effective on peak blasting pressures that occurred at carrier systems of RC buildings, although it is not effective on peak blasting pressures of infill walls.

The peak pressure values were obtained with empirical formulas recommended by Brode (1955) and graphs given in UFC 3-340-02. The scaled distance (Z) was calculated as 0.171 because 100 kg of TNT explosive was considered 0.5 m away from the building models. Therefore, the peak pressures were determined as 135.70 MPa for empirical formulas and 82.00 MPa for UFC 3-340-02. Moreover, it

Table 5 Peak pressure values obtained from 100 kg TNT explosive

Peak pressures (MPa)								
	C25	C30	C35	C40	C45	C50	Brode	UFC 3–340-02
Model 1	83.85	83.39	83.12	78.88	81.49	74.45	135.70	82.00
Model 2	88.81	86.56	85.91	82.58	79.78	68.83		

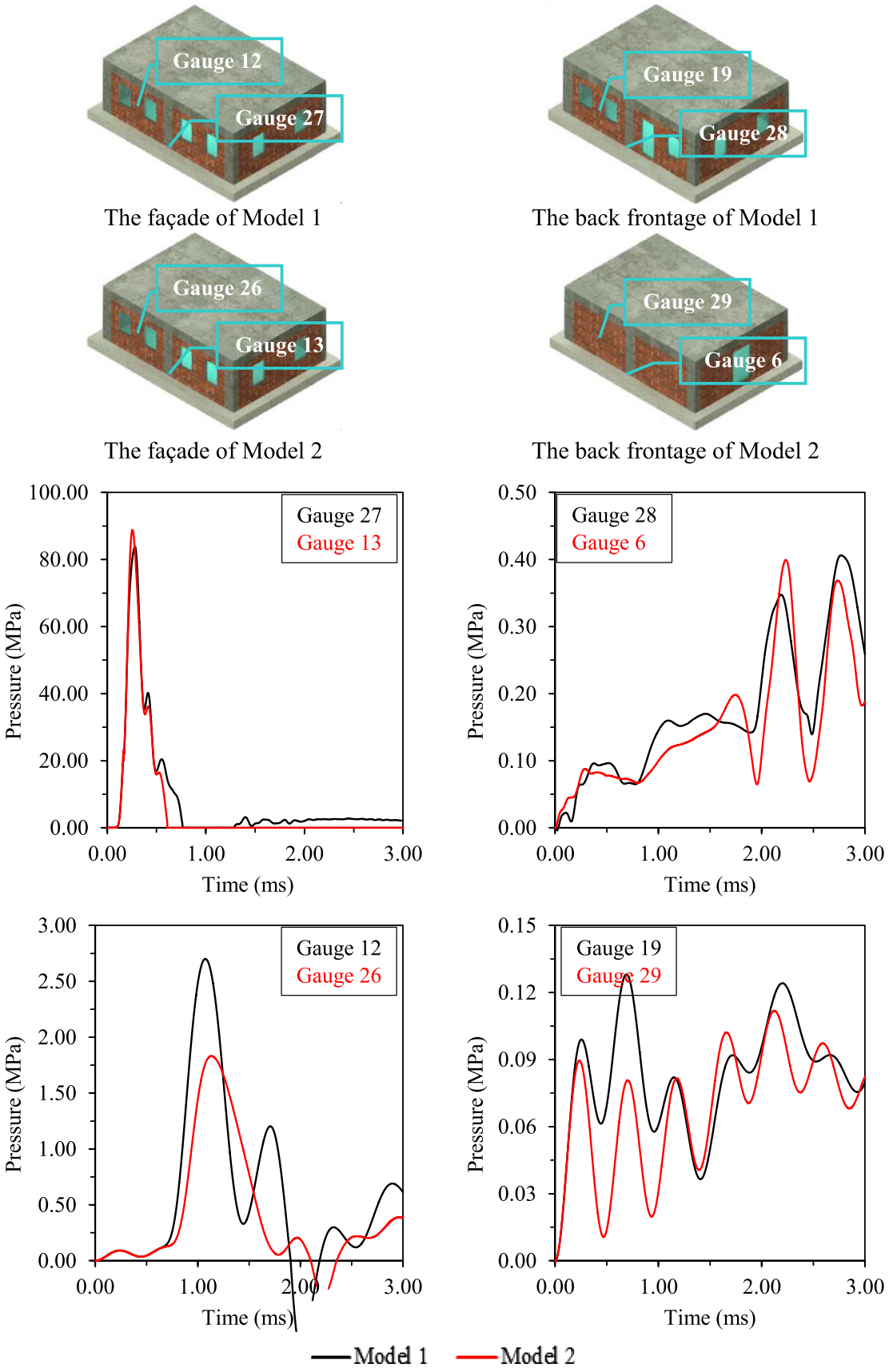

Fig. 18 The time-histories of pressures obtained from Model 1 and Model 2 for C25/30

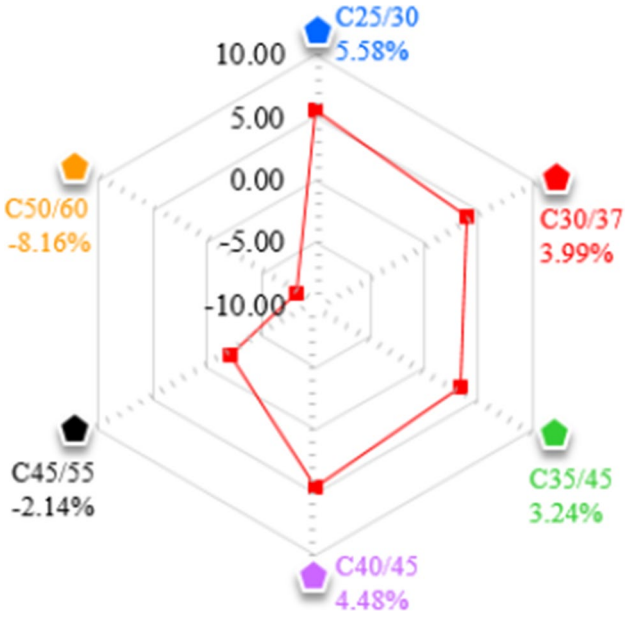

Fig. 19 The differences (%) in peak pressures of Model 2 due to the openings in infill walls according to the Model 1

was determined that the peak pressures obtained with UFC 3-340-02 are similar to the values determined by numerical methods. The peak pressures of selected building models obtained from 100 kg TNT explosive are given in Table 5.

On the other hand, the time-histories of pressures at all frontage for Model 1 and Model 2 are comparatively presented in Fig. 18 to determine the effects of infill wall openings on the blasting responses of the RC buildings. To this aim, the pressure C25/30 is considered. Also, the changes in peak pressures of Model 2 due to the openings in infill walls are shown in Fig. 19 for all concrete classes. It can be seen from Figs. 18 and 19 that the openings reduce the peak pressures of the infill walls contrary to the load-bearing system. The peak pressure of Model 2 increases 5.58% for C25/30, 3.99% for C30/37, 3.27% for C35/45, and 4.48% for C40/50, although it decreases 2.14% for C45/55 and 8.16% for C50/60, according to Model 1. In the literature, the infill walls which are regarded as the non-structural element and are directly exposed to blasting loads are generally evaluated for two perspectives: (1) a defense element against debris caused by explosion and (2) losses due to high-speed debris caused by damages or failures of the walls. Therefore, the contributions and effects of the infill walls and its opening on the blasting responses of the structures are generally neglected. However, the analysis results revealed that the peak pressures of carrier systems and infill walls are changed significantly due to opening in infill walls. Therefore, the roles of infill walls on the blasting behavior should be considered in the design and construction of structures that may be exposed to bursting loads.

The time-histories of displacements and contour diagrams of Model 1 and Model 2 are presented in Figs. 20, 21, 22 and 23, comparatively. Also, the maximum displacements and calculated differences for Model 1 and Model 2 with the increasing concrete strength (C25/30 referenced) are presented in Table 6 and Fig. 24. It can be seen from Figs. 20, 21, 22 and 23 that the gauges 27 and 13 for building models and gauges 12 and 27 for infill walls are critical in terms of displacements. These gauges are closest to the explosion center. The maximum displacements in Model 1 are calculated as 34.55 mm for C25/30, 32.82 mm for C30/37, 31.50 mm for C35/45, 28.72 mm for C40/50, 27.20 mm for C45/55, and 27.10 mm for C50/60. In similar to the Model 1, the maximum displacements in Model 2 decreased from 40.14 mm to 27.23 mm with the increasing concrete strength from C25/30 to C50/60.

It can be seen from Fig. 24 that maximum displacements decreased as 21.56% for Model 1 and 32.16% for Model 2 with the increasing of concrete strength. Moreover, the maximum displacements in the infill walls of Model 1 and Model 2 were found as 5.11 mm (gauge 12) and 4.75 mm (gauge 27) for all concrete classes, respectively. The results show that the concrete strength is considerably effective on maximum displacements of carrier systems, although it is not effective on maximum displacements of infill walls.

To determine the effects of infill wall openings on displacements, the time-histories of displacements at all frontage of Model 1 and Model 2 are presented in Fig. 25 for the C25/30 concrete class. Figure 26 presents the changes in maximum displacements of Model 2 compared to Model 1 due to the openings in infill walls for all concrete classes. According to Model 1, the maximum displacements in Model 2 increase 13.92% for C25/30, 11.98% for C30/37, 11.69% for C35/45, 10.80% for C40/50, 8.81% for C45/55, and 0.47% for C50/60. It can be seen from Figs. 25 and 26 that the maximum displacements in carrier systems and infill walls changed significantly due to opening in infill walls.

The released-total energy from the explosion, absorbed-total energy by the materials, and air volume are given in Table 7. It can be seen from Table 7, 3.6×10^{14} μJ of energy was released from 100 kg TNT explosive and a significant part of the released-energy was absorbed by the air volume (2.63×10^{14} μJ). However, the total

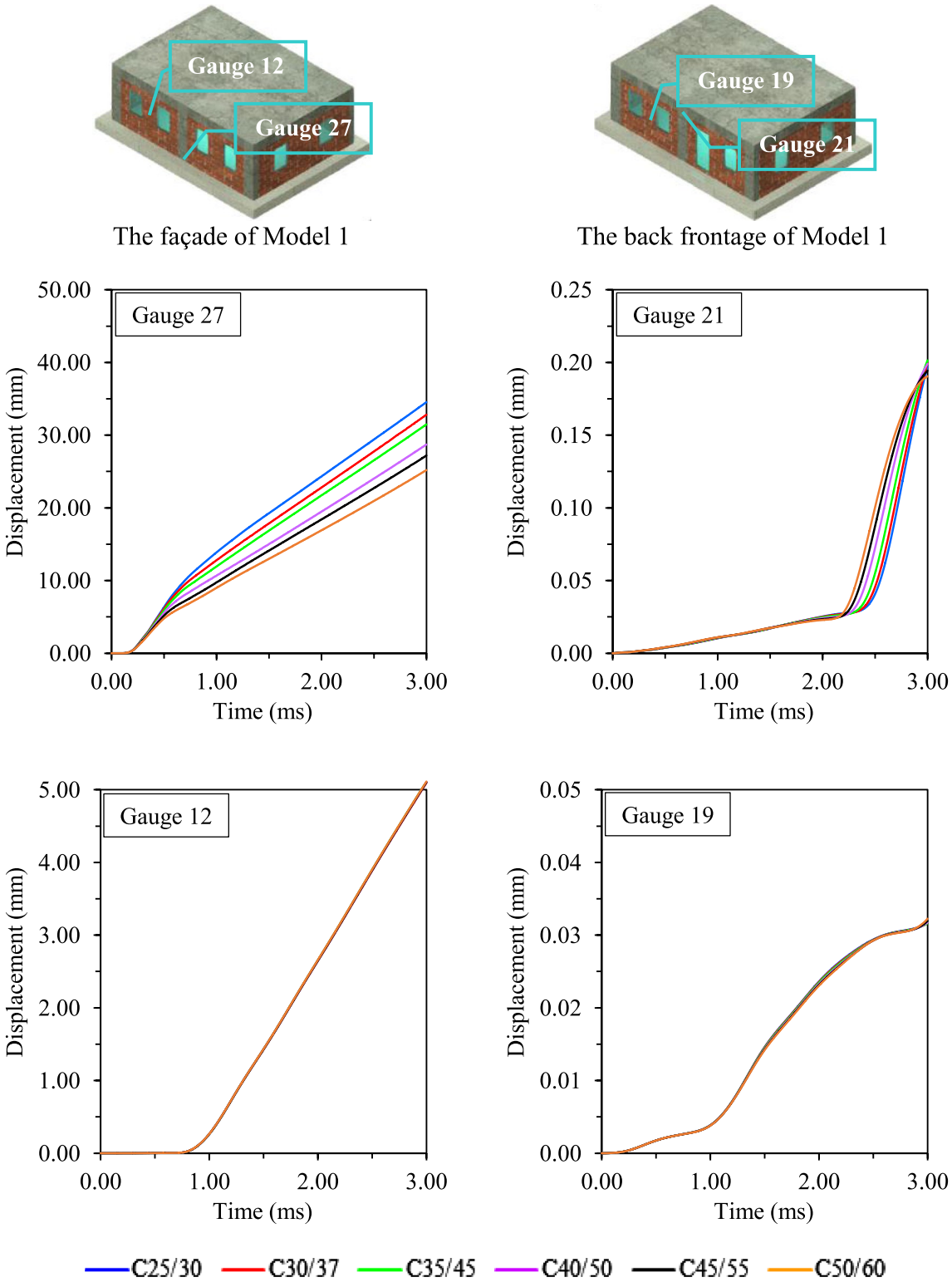

Fig. 20 The time-histories of displacements obtained from critical gauges of Model 1

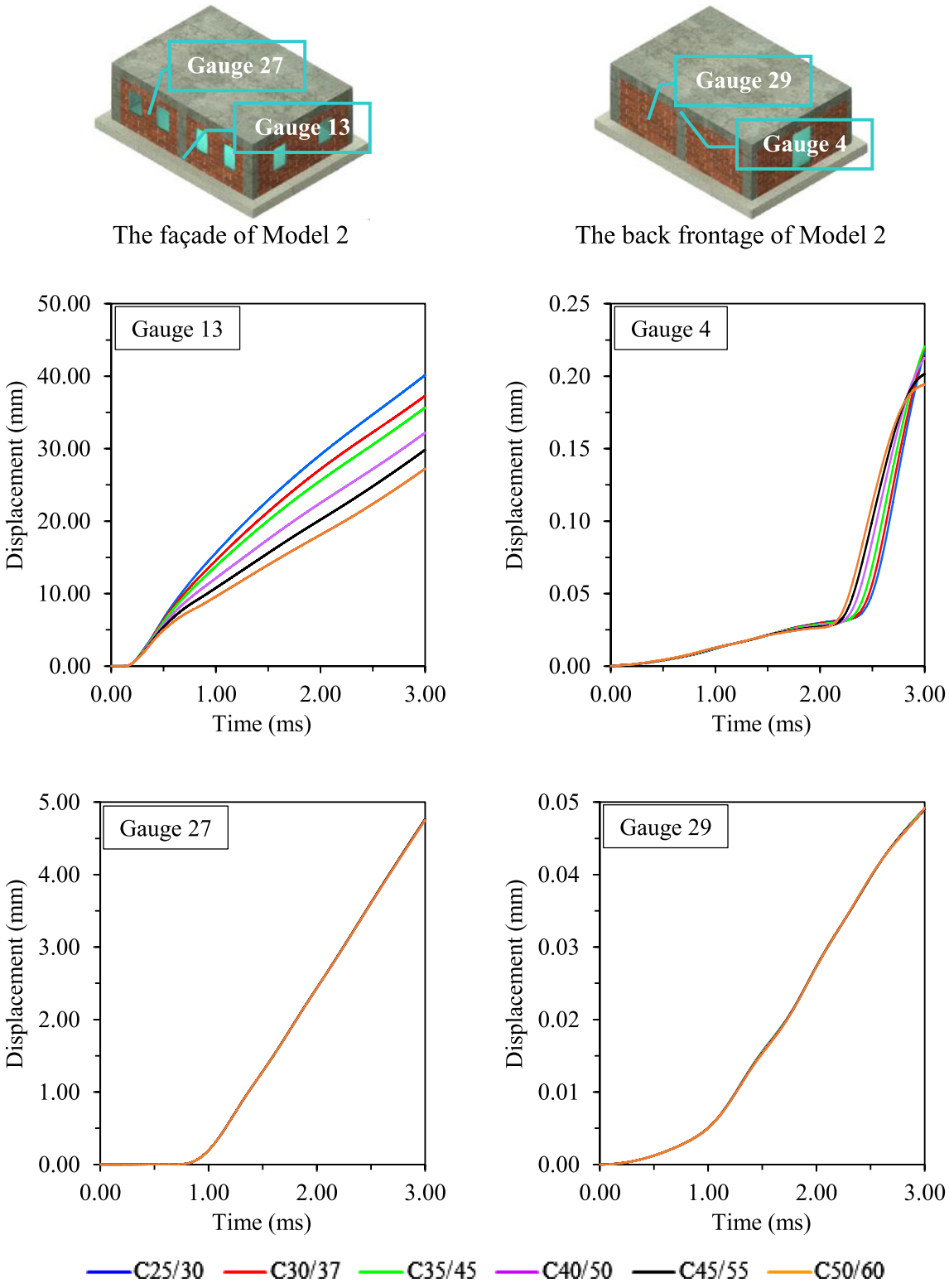

Fig. 21 The time-histories of displacements obtained from critical gauges of Model 2

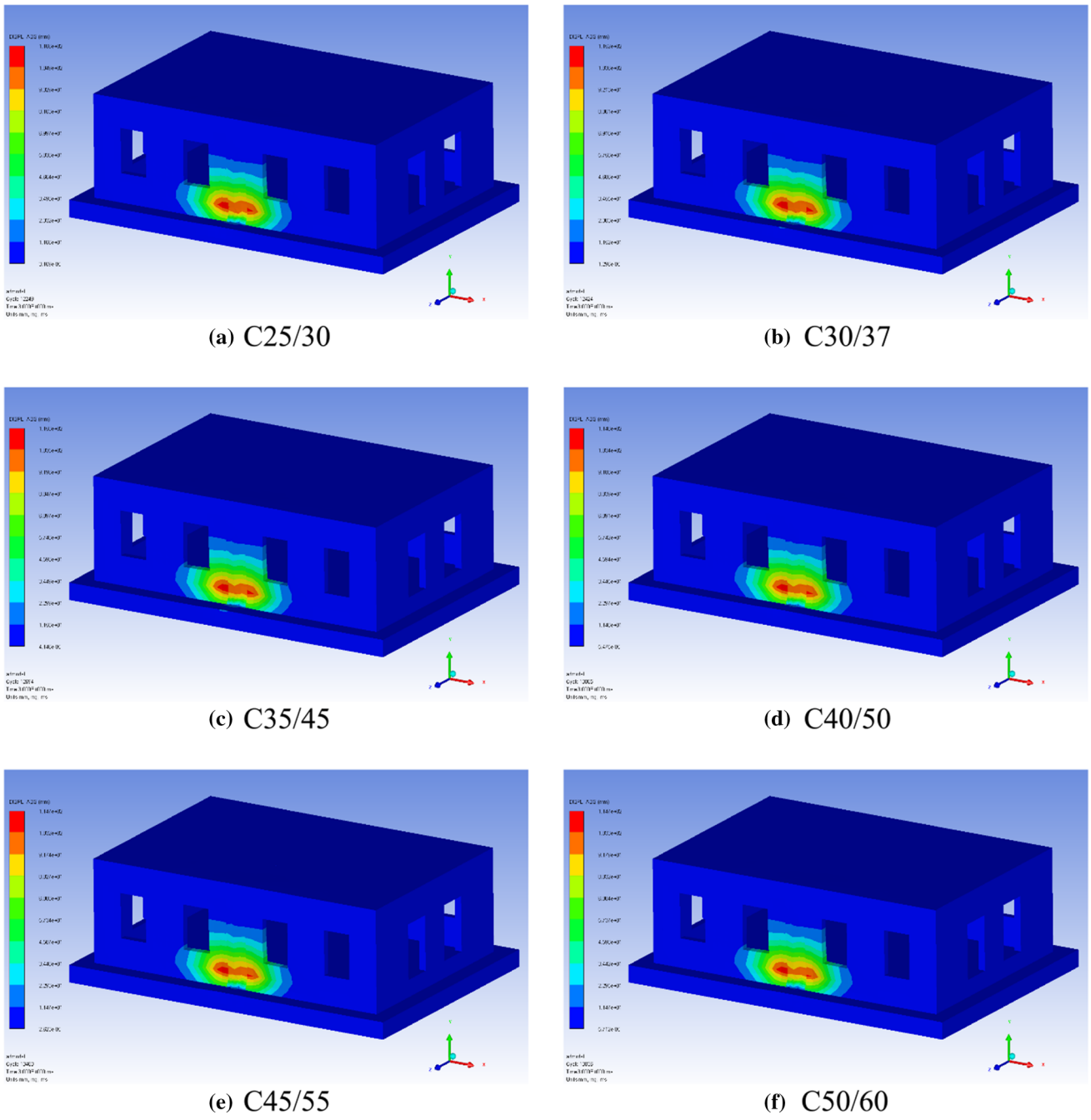

Fig. 22 The displacement contour diagrams obtained from 100 kg TNT explosive for Model 1

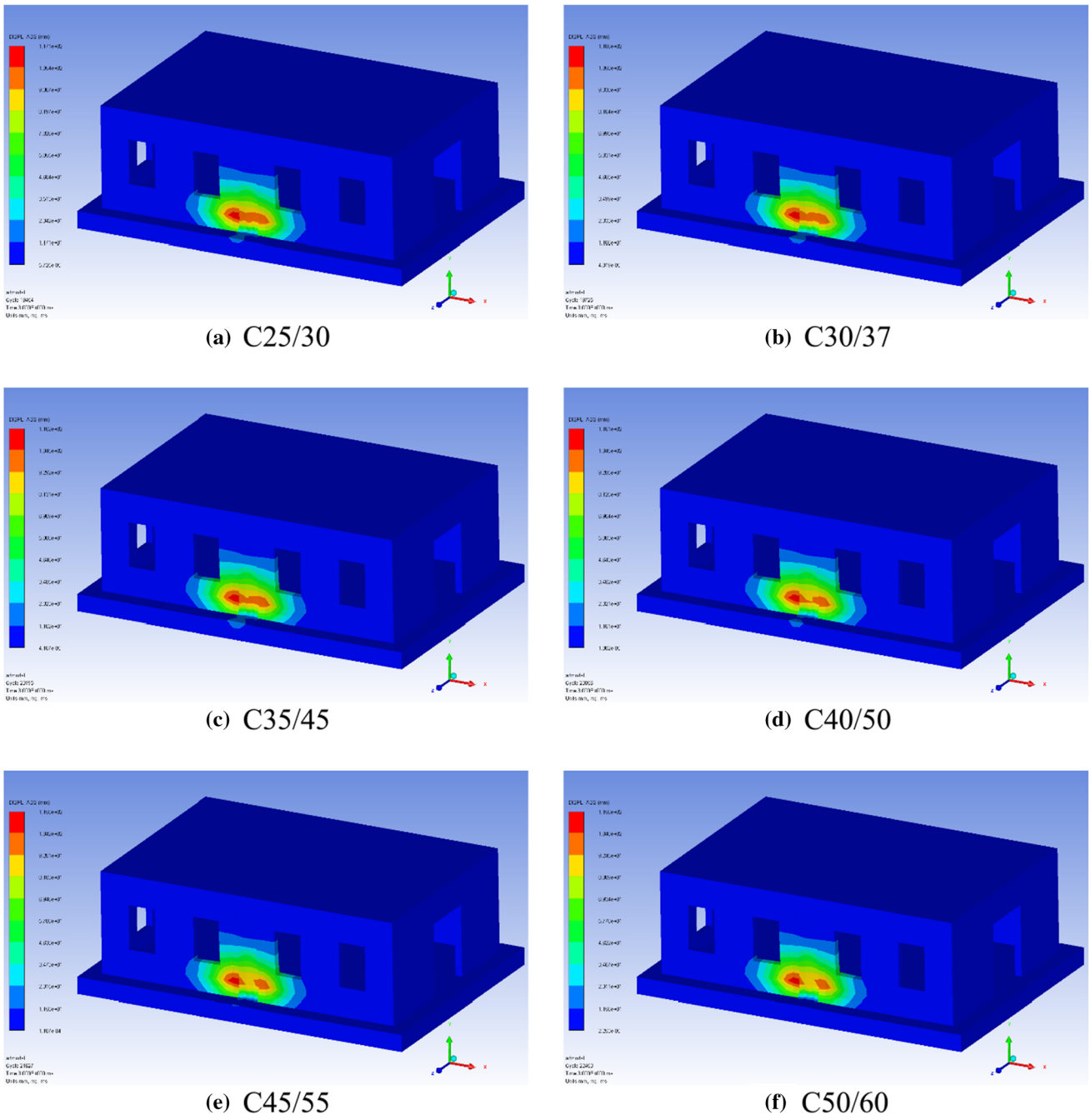

Fig. 23 The displacement contour diagrams obtained from 100 kg TNT explosive for Model 2

Table 6 Maximum displacements obtained from 100 kg TNT explosive

	Maximum displacements (mm)					
	C25	C30	C35	C40	C45	C50
Model 1	34.55	32.82	31.50	28.72	27.20	27.10
Model 2	40.14	37.29	35.67	32.20	29.83	27.23

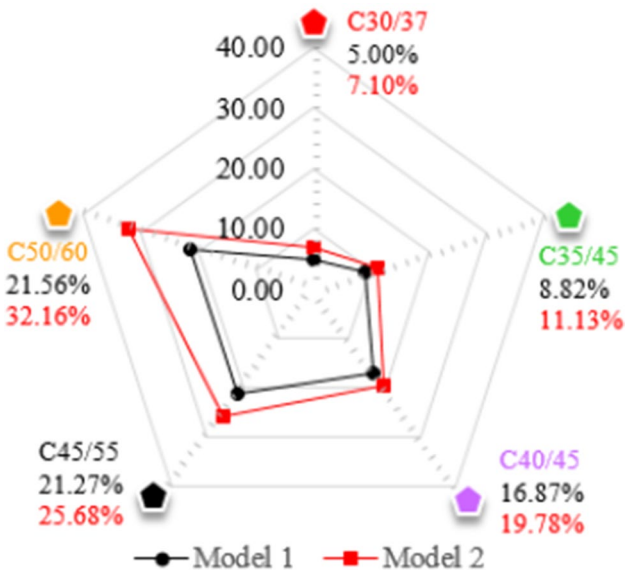

Fig. 24 The decreases (%) in maximum displacements of Model 1 and Model 2 with the concrete strength increasing from C25/30 to C50/60

released-energy was not absorbed by the air and other elements. Therefore, many elements were damaged. The energy absorbed by other solid elements (concrete, brick, etc.) is too small and can be neglected. Therefore, the concrete strength and openings on the infill walls have not significant effect on absorbed-total energy.

The damage contour diagrams obtained from blasting analyses are given in Figs. 27 and 28 for Model 1 and Model 2, respectively. It can be seen from Figs. 27 and 28 that damage distributions are similar for all blasting scenarios because the peak pressures caused by 100 kg TNT explosive are greater than the strength of the selected concrete classes and infill walls.

6 Conclusion

In this study, the effects of concrete strength and openings in infill walls on blasting responses of RC buildings are examined. For this purpose, in situ experimental tests were firstly conducted on a test specimen constructed with brick elements to verify the FE model. Moreover, two RC buildings were selected as an application and blasting analyses were performed by using numerical and empirical methods. The numerical models were constituted using ANSYS Workbench and were transferred into ANSYS AUTODYN to perform explicit analyses. In Model 1, openings were designed on the infill walls of all frontages so that the pressure caused by the explosion can easily enter and exit the building. In Model 2, the infill walls of the back frontage were considered as without openings. Moreover, C25/30 (f_{ck} = 25 MPa), C30/37 (f_{ck} = 30 MPa), C35/45 (f_{ck} = 35 MPa), C40/50 (f_{ck} = 40 MPa), C45/55 (f_{ck} = 45 MPa), and C50/60 (f_{ck} = 50 MPa) concrete classes were used in the analyses to investigate the concrete strength effect on blasting behavior. The pressures, displacements, damages, and total energies were considered as comparison parameters. By analyzing the results of the numerical and empirical studies, the following conclusions were obtained;

1. It was determined that the increase in concrete strength efficiently contributes to the blasting behavior of the load-bearing elements. As a result of the analyses, the peak pressure values in the load-bearing system decreased from 83.85 MPa to 74.45 MPa for Model 1 and 88.81 MPa to 68.83 MPa for Model 2 with the increasing concrete strength from C25/30 to C50/60. The peak pressures decrease by 11.21% for Model 1 and 22.50% for Model 2 with the increasing concrete strength.
2. The peak pressures in the infill walls of Model 1 and Model 2 were found as 2.70 MPa and 1.82 MPa for all concrete classes. This situation points out that the concrete strength is not effective on peak blasting pressures of infill walls.
3. The peak pressure values were obtained with empirical formulas. According to formulas recommended by Brode (1955) and graphs given in UFC 3-340-02, the peak pressures were calculated as 135.70 MPa and 82.00 MPa, respectively. Comparing the peak pressures obtained with numerical and analytical methods, it is apparent that the UFC 3-340-02 is similar to the FE results.
4. The maximum displacements decreased by 21.56% for Model 1 and 32.16% for Model 2 as the concrete strength increased from C25 / 30 to C50 / 60. The maximum and minimum displacements in Model 1 and Model 2 were obtained as 34.55 mm and 40.14 mm for C25/30, 27.10 mm and 27.23 mm for C50/60, respectively.

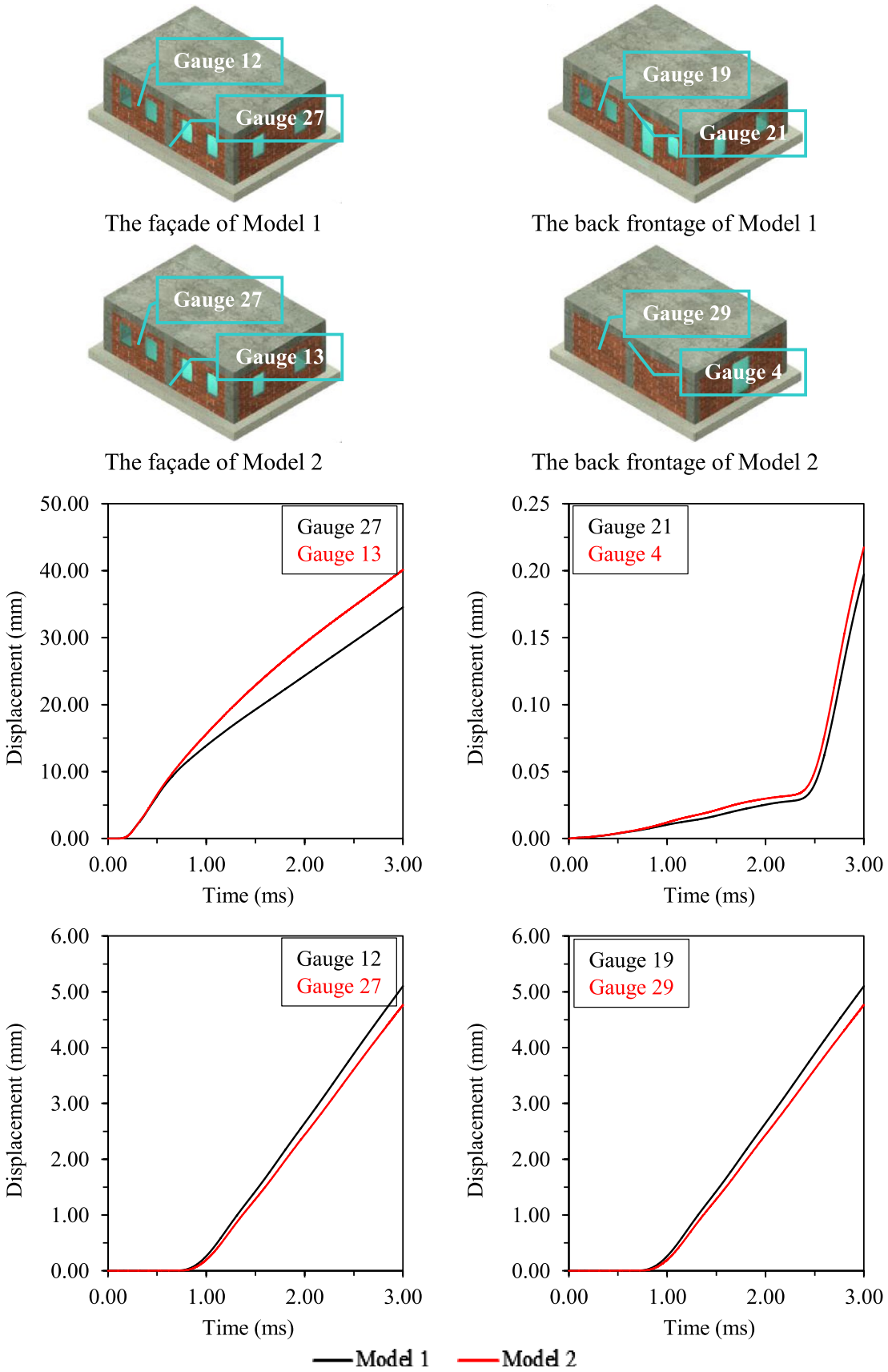

Fig. 25 The time-histories of displacements obtained Model 1 and Model 2 for C25/30

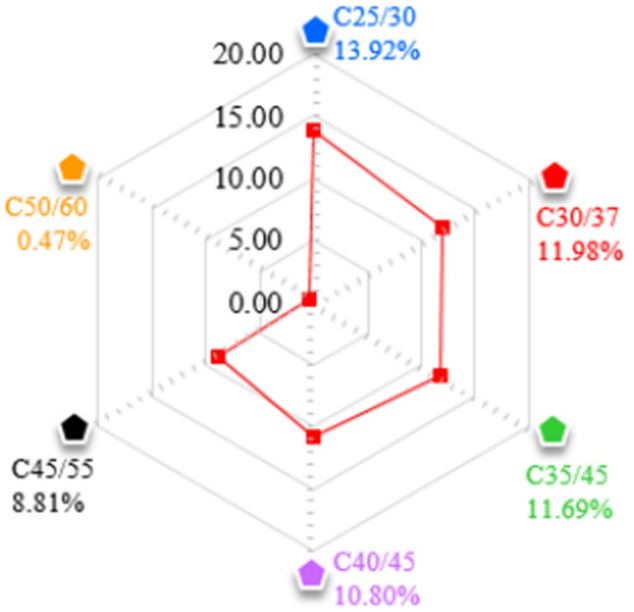

Fig. 26 The differences (%) in maximum displacements of Model 2 due to the openings in infill walls according to Model 1

5. The maximum displacements in the infill walls of Model 1 and Model 2 were found as 5.11 mm and 4.75 mm for all concrete classes. Similar to the peak pressure, the concrete strength is not effective on displacements of infill walls.
6. It is seen that the openings in infill walls lead to a change of 8.16% in peak pressures and 13.92% in maximum displacements. It is apparent that the peak pressures and maximum displacements of carrier systems and infill walls are changed significantly due to opening in infill walls.
7. It has been determined that the critical gauge points at which maximum structural responses are obtained in both the load-bearing system and the infill walls are the closest points to the explosion center.
8. It is observed from numerical analyses that a significant part of the released-energy from the explosion was absorbed by the air volume and the energy absorbed by other solid elements can be neglected. Since the total released-energy was not absorbed by the elements, many structural and non-structural elements were damaged.

Although the explosions caused by terrorism and/or accidental lead to serious damage and/or collapse in structures, explosion effects are generally neglected in the design stage of civil engineering structures. However, all comparisons show that the concrete strength and openings in infill walls are significantly effective on the blasting responses of RC buildings. Therefore, explosion-resistant structures can be designed using at least these parameters. The study can be extended with the following issues;

1. For strategically important civil engineering structures such as buildings and bridges, studies can be conducted on city development plans and building layouts that can reduce blasting effects.
2. The parametric studies using multiple variables can be done to examine the effects of various parameters such as charge weights and load-bearing types that can be used in explosion-proof building design.
3. The blasting responses and blastwave effects on the structures can be investigated by using detailed numerical models including various interactions such as soil–structure, load-bearing system-wall, and walls-mortar. Thus, the effects of these interactions on blasting behavior can be investigated.

Table 7 The released-total energy and absorbed-total energy after detonation

		Total energy (μJ) ($\times 10^{10}$)					
		C25	C30	C35	C40	C45	C50
Model 1	Concrete	118.00	115.00	110.00	104.00	98.05	92.90
	Reinforcing steel	2.56	2.52	2.47	2.39	2.31	2.27
	Wall	58.60	58.80	58.80	58.60	58.59	58.50
	Air	26,300.00					
	TNT	36,000.00					
Model 2	Concrete	122.00	118.00	114.00	110.00	101.30	96.70
	Reinforcing steel	4.03	3.90	3.77	3.59	3.41	3.32
	Wall	58.90	58.90	58.80	58.90	58.77	58.80
	Air	26,300.00					
	TNT	36,000.00					

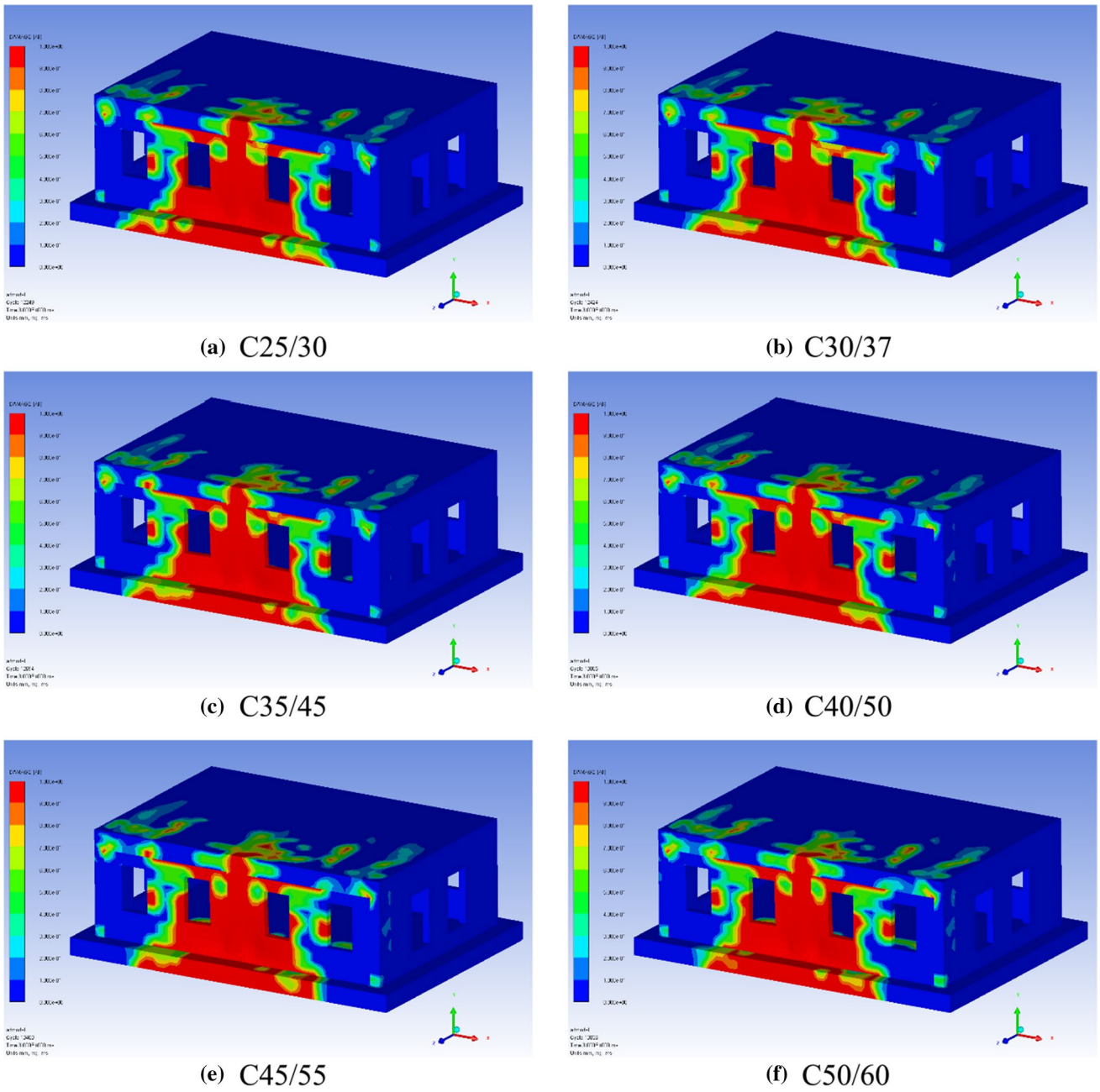

Fig. 27 The damage contour diagrams obtained from 100 kg TNT explosive for Model 1

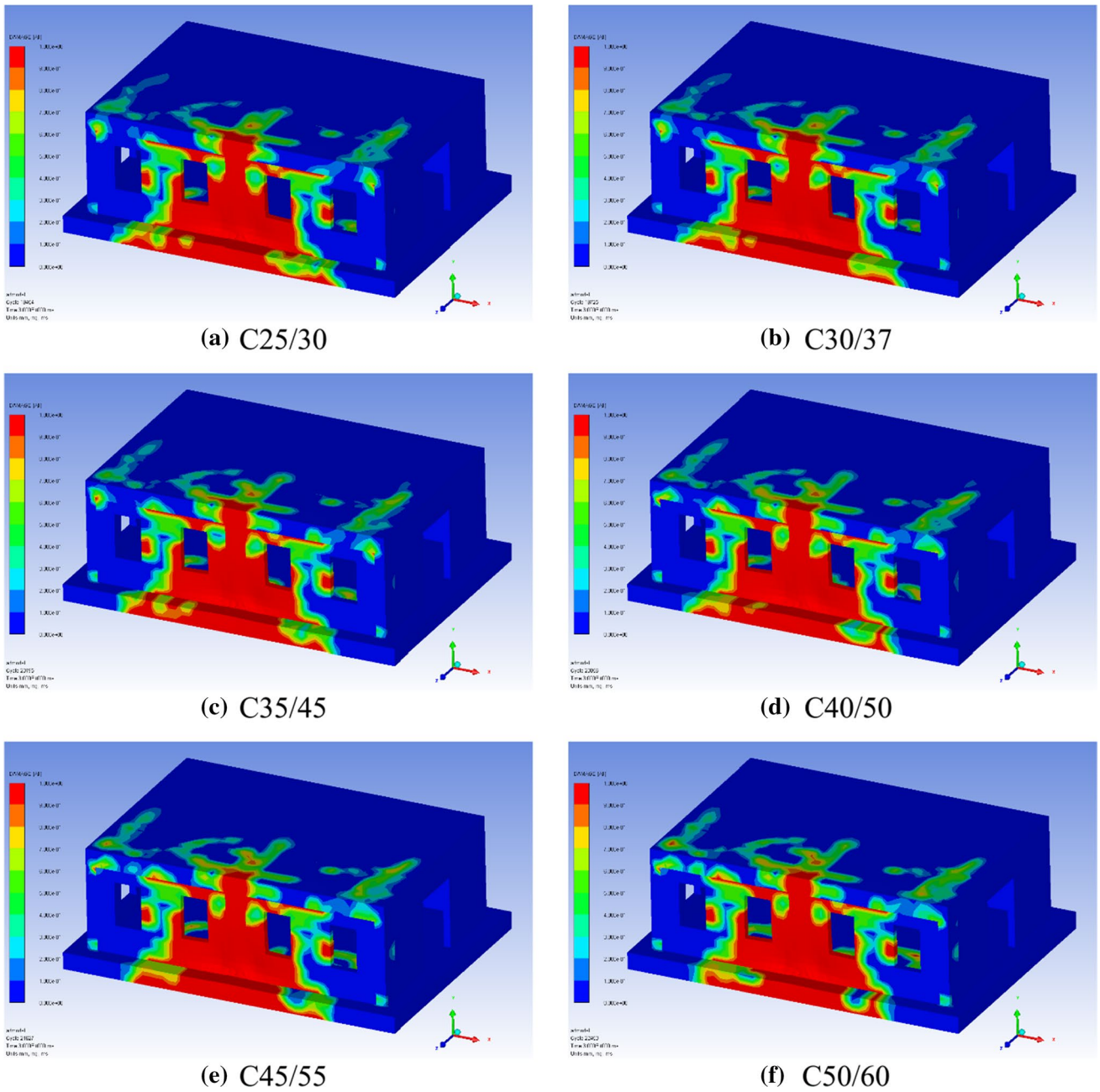

Fig. 28 The damage contour diagrams obtained from 100 kg TNT explosive for Model 2

References

Al Hanoun MH, Abrahamczyk L, Schwarz J (2018) Macromodeling of in- and out-of-plane behavior of unreinforced masonry infill walls. Bull Earthq Eng 17(1):519–535. https://doi.org/10.1007/s10518-018-0458-x

Alsayed SH, Elsanadedy HM, Al-Zaheri ZM, Al-Salloum YA, Abbas H (2016) Blast response of GFRP-strengthened infill masonry walls. Constr Build Mater 115:438–451. https://doi.org/10.1016/j.conbuildmat.2016.04.053

Altunlu, K. (2008) Safety assessment of r/c columns against explosive attacks by vehicle or human from exterior (Master's thesis)

Andreou M, Kotsoglou A, Pantazopoulou S (2016) Modelling blast effects on a reinforced concrete bridge. Adv Civ Eng 2016:1–11. https://doi.org/10.1155/2016/4167329

ANSYS AUTODYN, (2016) Swanson Analyses System. Ansys Inc, USA

Workbench ANSYS (2016) Swanson analyses system. Ansys Inc, USA

Aoude H, Dagenais FP, Burrell RP, Saatcioglu M (2015) Behavior of ultra-high performance fiber reinforced concrete columns under blast loading. Int J Impact Eng 80:185–202. https://doi.org/10.1016/j.ijimpeng.2015.02.006

Brode HL (1955) Numerical solutions of spherical blast waves. J Appl Phys 26(6):766–775

Cavaleri L, Zizzo M, Asteris PG (2020) Residual out-of-plane capacity of infills damaged by in-plane cyclic loads. Eng Struct 209:109957. https://doi.org/10.1016/j.engstruct.2019.109957

Chen Y, Wang B, Zhang B, Zheng Q, Zhou J, Jin F, Fan H (2020) Polyurea coating for foamed concrete panel: an efficient way to resist explosion. Def Technol 16(1):136–149. https://doi.org/10.1016/j.dt.2019.06.010

Codina R, Ambrosini D, de Borbon F (2017) Alternatives to prevent progressive collapse protecting reinforced concrete columns subjected to near field blast loading. Proc Eng 199:2445–2450. https://doi.org/10.1016/j.proeng.2017.09.380

Coffield A, Adeli H (2015) Irregular steel building structures subjected to blast loading. J Civ Eng Manag 22(1):17–25. https://doi.org/10.3846/13923730.2015.1073172

Davidson JS, Porter JR, Dinan RJ, Hammons MI, Connell JD (2004) Explosive testing of polymer retrofit masonry walls. J Perform Constr Facil 18(2):100–106. https://doi.org/10.1061/(asce)0887-3828(2004)18:2(100)

De Risi MT, Di Domenico M, Ricci P, Verderame GM, Manfredi G (2019) Experimental investigation on the influence of the aspect ratio on the in-plane/out-of-plane interaction for masonry infills in RC frames. Eng Struct 189:523–540. https://doi.org/10.1016/j.engstruct.2019.03.111

Di Domenico M, Ricci P, Verderame GM (2019) Experimental assessment of the out-of-plane strength of URM infill walls with different slenderness and boundary conditions. Bull Earthq Eng 17(7):3959–3993. https://doi.org/10.1007/s10518-019-00604-5

Furtado A, Rodrigues H, Arêde A, Varum H (2015) Experimental characterization of the in-plane and out-of-plane behaviour of infill masonry walls. Proc Eng 114:862–869. https://doi.org/10.1016/j.proeng.2015.08.041

Furtado A, Rodrigues H, Varum H, Arêde A (2018) Mainshock-aftershock damage assessment of infilled RC structures. Eng Struct 175:645–660. https://doi.org/10.1016/j.engstruct.2018.08.063

Furtado A, Rodrigues H, Arêde A, Varum H (2020) Effect of the panel width support and columns axial load on the infill masonry walls out-of-plane behavior. J Earthquake Eng 24(4):653–681. https://doi.org/10.1080/13632469.2018.1453400

Hacıefendioğlu K, Koç V (2016) Dynamic assessment of partially damaged historic masonry bridges under blast-induced ground motion using multi-point shock spectrum method. Appl Math Model 40(23–24):10088–10104. https://doi.org/10.1016/j.apm.2016.06.049

Hacıefendioğlu K (2017) Stochastic dynamic response of short-span highway bridges to spatial variation of blasting ground vibration. Appl Math Comput 292:194–209. https://doi.org/10.1016/j.amc.2016.07.039

Hao H, Tang EKC (2010) Numerical simulation of a cable-stayed bridge response to blast loads, part II: Damage prediction and FRP strengthening. Eng Struct 32(10):3193–3205. https://doi.org/10.1016/j.engstruct.2010.06.006

Hashemi SK, Bradford MA, Valipour HR (2017) Dynamic response and performance of cable-stayed bridges under blast load: effects of pylon geometry. Eng Struct 137:50–66. https://doi.org/10.1016/j.engstruct.2017.01.032

Henrych J, Major R (1979) The dynamics of explosion and its use. Elsevier, Amsterdam

Herrmann W (1969) Constitutive equation for the dynamic compaction of ductile porous materials. J Appl Phys 40(6):2490–2499

Hopkinson B, Cranz C (1915). Cube root scaling law

Jayasooriya R, Thambiratnam DP, Perera NJ, Kosse V (2011) Blast and residual capacity analysis of reinforced concrete framed buildings. Eng Struct 33(12):3483–3495. https://doi.org/10.1016/j.engstruct.2011.07.011

Johnson GR, Cook WH (1983). A constitutive model and data for metals subjected to large strains, high strain rates and high temperatures. In proceedings of the 7th international symposium on ballistics. vol. 21, no. 1, pp 541–547

Kelliher D, Sutton-Swaby K (2012) Stochastic representation of blast load damage in a reinforced concrete building. Struct Saf 34(1):407–417. https://doi.org/10.1016/j.strusafe.2011.08.001

Keys RA, Clubley SK (2017) Establishing a predictive method for blast induced masonry debris distribution using experimental and numerical methods. Eng Fail Anal 82:82–91. https://doi.org/10.1016/j.engfailanal.2017.07.017

Kingery CN, Bulmash G (1984) Air blast parameters from TNT spherical air burst and hemispherical burst, Technical Report ARBRL-TR-02555: AD-B082 713. U.S, Army Ballistic Research Laboratory, Aberdeen Proving Ground, MD

Kinney GF, Graham KJ (1985) Explosive shocks in air. Springer, Berlin Germany

Li Z, Chen L, Fang Q, Hao H, Zhang Y, Xiang H, Chen W, Yang S, Bao Q (2017) Experimental and numerical study of unreinforced clay brick masonry walls subjected to vented gas explosions. Int J Impact Eng 104:107–126. https://doi.org/10.1016/j.ijimpeng.2017.02.002

Luccioni BM, Ambrosini RD, Danesi RF (2004) Analysis of building collapse under blast loads. Eng Struct 26(1):63–71. https://doi.org/10.1016/j.engstruct.2003.08.011

Mills CA (1987) The design of concrete structures to resist explosions and weapon effects. In proceedings of the 1st international conference on concrete for hazard protections, Edinburgh, UK.

Ngo T, Mendis P, Gupta A, Ramsay J (2007) Blast loading and blast effects on structures–an overview. Electr J Struct Eng 7(S1):76–91

Onat O, Correia AA, Lourenço PB, Koçak A (2018) Assessment of the combined in-plane and out-of-plane behavior of brick infill walls within reinforced concrete frames under seismic loading. Earthq Eng Struct Dynam 47(14):2821–2839. https://doi.org/10.1002/eqe.3111

Onat O (2019) Experimental damage evaluation of prototype infill wall based on forced vibration test. Adv Concr Constr 8(2):77–90. https://doi.org/10.12989/acc.2019.8.2.077

Ricci P, Di Domenico M, Verderame GM (2020) Effects of the in-plane/out-of-plane interaction in urm infills on the seismic performance of rc buildings designed to Eurocodes. J Earthq Eng. https://doi.org/10.1080/13632469.2020.1733137

Riedel W, Thoma K, Hiermaier S, Schmolinske E (1999) Penetration of reinforced concrete by BETA-B-500 numerical analysis using a new macroscopic concrete model for hydrocodes. In: Proceedings of the 9th international symposium on the effects of munitions with structures. Vol. 315. Berlin-Strausberg, Germany.

Sadovsky MA (2004) Mechanical effects of air shockwaves from explosions according to experiments. Geophysics and physics of explosion. Nauka Press, Moscow Russia

Sevim B, Toy AT (2019) Blasting response of a two-storey rc building under different charge weight of TNT explosives. Iran J Sci Technol Trans Civ Eng 44(2):565–577. https://doi.org/10.1007/s40996-019-00256-0

Shi Y, Xiong W, Li Z-X, Xu Q (2016) Experimental studies on the local damage and fragments of unreinforced masonry walls under close-in explosions. Int J Impact Eng 90:122–131. https://doi.org/10.1016/j.ijimpeng.2015.12.002

Son J, Lee H-J (2011) Performance of cable-stayed bridge pylons subjected to blast loading. Eng Struct 33(4):1133–1148. https://doi.org/10.1016/j.engstruct.2010.12.031

Tan KH, Patoary MKH (2009) Blast resistance of frp-strengthened masonry walls. I: approximate analysis and field explosion tests. J Comp Constr 13(5):422–430. https://doi.org/10.1061/(asce)1090-0268(2009)13:5(422)

Tang EKC, Hao H (2010) Numerical simulation of a cable-stayed bridge response to blast loads, part I: Model development and response calculations. Eng Struct 32(10):3180–3192. https://doi.org/10.1016/j.engstruct.2010.06.007

TEC (2018) Turkish earthquake code. Disaster and Emergency Management Presidency, Ankara, Turkey

Toy AT, Sevim B (2017) Numerically and empirically determination of blasting response of a RC retaining wall under TNT explosive. Adv Concr Constr 5(5):493–512. https://doi.org/10.12989/acc.2017.5.5.493

TS500. (2000) Requirements for design and construction of reinforced concrete structures. Institute of Turkish Standard, Ankara, Turkey

UFC 3–340-02, (2008) Unified facilities criteria: structures to resist the effects of accidental explosions. Department of Defense, Washington, USA

Ullah A, Ahmad F, Jang H-W, Kim S-W, Hong J-W (2017) Review of analytical and empirical estimations for incident blast pressure. KSCE J Civ Eng 21(6):2211–2225. https://doi.org/10.1007/s12205-016-1386-4

Wei X, Stewart MG (2010) Model validation and parametric study on the blast response of unreinforced brick masonry walls. Int J Impact Eng 37(11):1150–1159. https://doi.org/10.1016/j.ijimpeng.2010.04.003

Wu C, Hao H, Lu Y, Sun S (2004) Numerical simulation of structural responses on a sand layer to blast induced ground excitations. Comput Struct 82(9–10):799–814. https://doi.org/10.1016/j.compstruc.2004.01.003

Wu C, Hao H, Lu Y (2005) Dynamic response and damage analysis of masonry structures and masonry infilled RC frames to blast ground motion. Eng Struct 27(3):323–333. https://doi.org/10.1016/j.engstruct.2004.10.004

Yalciner H (2014) Structural response to blast loading: the effects of corrosion on reinforced concrete structures. Shock Vib 2014:1–7. https://doi.org/10.1155/2014/529892

Yusof MA, Rosdi RN, Nor NM, Ismail A, Yahya MA, Peng NC (2014) Simulation of reinforced concrete blast wall subjected to air blast loading. J Asian sci Res 4(9):522–533

Zapata BJ, Weggel DC (2008) Collapse Study of an unreinforced masonry bearing wall building subjected to internal blast loading. J Perform Constr Facil 22(2):92–100. https://doi.org/10.1061/(asce)0887-3828(2008)22:2(92)

Zhang R, Phillips BM (2016) Performance and protection of base-isolated structures under blast loading. J Eng Mech 142(1):04015063. https://doi.org/10.1061/(asce)em.1943-7889.0000974